FINAL REPORT
U.S.ARMY GRANT DAAG29-80-K-0058
"Mechanics of the Removal of Thickened Chemical Agents
from Contaminated Surfaces by Wiping"

THEORETICAL AND EXPERIMENTAL STUDIES OF WIPING WITH A RIGID BLADE

Timothy M. Sullivan and Stanley Middleman

Department of Applied Mechanics and Engineering Sciences
University of California, San Diego
La Jolla, California 92093

January 20, 1985

Unclassified

SECURITY CLASSIFICATION OF THIS PAGE (When Data Entered)

REPORT DOCUMENTATION PAGE		READ INSTRUCTIONS BEFORE COMPLETING FORM
1. REPORT NUMBER ARO 17226.2-EG	2. GOVT ACCESSION NO.	3. RECIPIENT'S CATALOG NUMBER
4. TITLE (and Subtitle) MECHANICS OF THE REMOVAL OF THICKENED CHEMICAL AGENTS FROM CONTAMINATED SURFACES BY WIPING		5. TYPE OF REPORT & PERIOD COVERED Final Report 08-01-80 through 10-31-84 6. PERFORMING ORG. REPORT NUMBER
7. AUTHOR(s) Timothy M. Sullivan Stanley Middleman		8. CONTRACT OR GRANT NUMBER(s) DAAG29-80-K-0058
9. PERFORMING ORGANIZATION NAME AND ADDRESS University of California, San Diego Applied Mechanics & Engineering Sciences, B-010 La Jolla, California 92093		10. PROGRAM ELEMENT, PROJECT, TASK AREA & WORK UNIT NUMBERS
11. CONTROLLING OFFICE NAME AND ADDRESS U. S. Army Research Office Post Office Box 12211 Research Triangle Park, NC 27709		12. REPORT DATE 01-20-85 13. NUMBER OF PAGES 85
14. MONITORING AGENCY NAME & ADDRESS(if different from Controlling Office)		15. SECURITY CLASS. (of this report) Unclassified 15a. DECLASSIFICATION/DOWNGRADING SCHEDULE

16. DISTRIBUTION STATEMENT (of this Report)

Approved for public release; distribution unlimited.

17. DISTRIBUTION STATEMENT (of the abstract entered in Block 20, if different from Report)

18. SUPPLEMENTARY NOTES

The view, opinions, and/or findings contained in this report are those of the author(s) and should not be construed as an official Department of the Army position, policy, or decision, unless so designated by other documentation

19. KEY WORDS (Continue on reverse side if necessary and identify by block number)

Wiping, Chemical Contaminant, Surface, Viscoelastic Fluid, Lubrication Theory, Elastic Effects.

20. ABSTRACT (Continue on reverse side if necessary and identify by block number)

The process of wiping a thickened chemical contaminant from a surface, where it has been inadvertantly transferred and may pose a safety hazard, is investigated with regard to the fundamental fluid mechanics. Of special interest is the effect viscoelastic fluid behavior has on the process and specifically the amount of fluid remaining after wiping. Rigid aluminum blades of variable geometry, accurately positioned above a smooth rotating cylindrical surface, provide an experimental model of the process. Residual fluid thickness data as a function of blade height for newtonian liquids are compared to a simple lubrication theory model, while a

DD FORM 1 JAN 73 1473 EDITION OF 1 NOV 65 IS OBSOLETE

UNCLASSIFIED

SECURITY CLASSIFICATION OF THIS PAGE (When Data Entered)

more thorough Finite Element solution to the problem is planned for the future. Preliminary results indicate the potential to separate shear thinning and elastic effects experimentally through the proper choice of test fluids.

TABLE OF CONTENTS

ABSTRACT

The process of wiping a thickened chemical contaminant from a surface, where it has been inadvertantly transferred and may pose a safety hazard, is investigated with regard to the fundamental fluid mechanics. Of special interest is the effect viscoelastic fluid behavior has on the process and specifically the amount of fluid remaining after wiping . Rigid aluminum blades of variable geometry, accurately positioned above a smooth rotating cylindrical surface, provide an experimental model of the process. Residual fluid thickness data as a function of blade height for newtonian liquids are compared to a simple lubrication theory model, while a more thorough Finite Element solution to the problem is planned for the future. Preliminary results indicate the potential to separate shear thinning and elastic effects experimentally through the proper choice of test fluids.

INTRODUCTION

The process of wiping a contaminating fluid from a surface poses an interesting fluid dynamics problem and is of practical interest as well. Although a wiping step alone is rarely sufficient to render a surface "clean", optimizing the wiping process (minimizing the amount of contaminant remaining) can considerably reduce the requirements of additional, more costly, cleaning processes.

A simple geometry for investigating the wiping process is shown in Figure 1. Hsu (1984) considers a similar geometry to study the the forces generated in a blade coating process. His analysis is the basis for a simple analytical model presented here, with two modifications. First, his primary interest is in the pressure field generated under the blade, while we are concerned with the amount of liquid left behind after the wiping process. Secondly, he considers only a specific case of our more generalized geometry, leaving open the question of how sensitive the results are to blade orientation and placement. Following Hsu, a perturbation method is used to obtain an analytical solution for newtonian liquids, and justification is given for retaining only the zeroth order solution (equivalent to lubrication theory - Cameron, 1966). A specially designed wiping apparatus is used to collect residual fluid thickness data, for comparison. Data for newtonian liquids show good agreement with the model under some conditions, and provide insight into

the limitations of the model under others.

The model is extended to purely viscous non-newtonian liquids, by incorporating a shear dependent viscosity function into the equations. Experiments with viscoelastic liquids demonstrate that the residual fluid thickness can differ markedly from values predicted by lubrication theory for purely viscous fluids.

ANALYTICAL SOLUTIONS

Newtonian Liquids:

Figure 2 gives a definition sketch for the geometry and coordinates. We start with the steady state Navier-Stokes equations (neglecting gravity) in two dimensions, written in cartesian coordinates as

$$\rho\left(u\frac{\partial u}{\partial x}+v\frac{\partial u}{\partial y}\right)=-\frac{\partial p}{\partial x}+\mu\frac{\partial^2 u}{\partial x^2}+\mu\frac{\partial^2 u}{\partial y^2} \tag{1}$$

$$\rho\left(u\frac{\partial v}{\partial x}+v\frac{\partial v}{\partial y}\right)=-\frac{\partial p}{\partial y}+\mu\frac{\partial^2 v}{\partial x^2}+\mu\frac{\partial^2 v}{\partial y^2} \tag{2}$$

The continuity equation is

$$\frac{\partial u}{\partial x}+\frac{\partial v}{\partial y}=0 \tag{3}$$

We nondimensionalize the variables with a set of scaling factors as follows:

$$\phi=\frac{u}{U} \qquad \xi=\frac{x}{L_x}$$

$$\psi=\frac{v}{V} \qquad \eta=\frac{y}{\bar{h}}$$

$$\pi=\frac{p}{P}$$

For the time, we leave U, $\bar{h}$, and L_x undefined with respect to

the specific system (the wiper) of interest, but specify that

$$V = \frac{U\bar{h}}{L_x} \qquad P = \frac{\mu U L_x}{\bar{h}^2}$$

We define a Reynolds number (Re) as

$$Re = \frac{\rho U \bar{h}^2}{\mu L_x}$$

and a geometrical parameter α as

$$\alpha = \left(\frac{\bar{h}}{L_x}\right)^2$$

Then Eqs. 1-3 become

$$Re\left(\phi \frac{\partial \phi}{\partial \xi} + \psi \frac{\partial \phi}{\partial \eta}\right) = -\frac{\partial \pi}{\partial \xi} + \frac{\partial^2 \phi}{\partial \eta^2} + \alpha \frac{\partial^2 \phi}{\partial \xi^2} \tag{4}$$

$$\alpha Re\left(\phi \frac{\partial \psi}{\partial \xi} + \psi \frac{\partial \psi}{\partial \eta}\right) = -\frac{\partial \pi}{\partial \eta} + \alpha^2 \frac{\partial^2 \psi}{\partial \xi^2} + \alpha \frac{\partial^2 \psi}{\partial \eta^2} \tag{5}$$

$$\frac{\partial \phi}{\partial \xi} + \frac{\partial \psi}{\partial \eta} = 0 \tag{6}$$

It is useful to rewrite Eq. 6 as

$$\psi = -\int_{\sigma(\xi)}^{\beta(\xi)} \frac{\partial \phi}{\partial \xi}\, d\eta + \psi_\sigma \tag{7}$$

Boundary conditions for the wiper take the forms of the following

equations (see Fig. 2)

$$\phi = 0 \quad \text{and} \quad \Psi = 0 \qquad \text{on} \quad \eta = \beta(\xi) \tag{8}$$

$$\phi = \phi_0(\xi) \quad \text{and} \quad \Psi = \phi_0 \frac{\partial \sigma}{\partial \xi} \qquad \text{on} \quad \eta = \sigma(\xi) \tag{9}$$

$$\pi = 0 \qquad \text{on} \quad \xi = \xi_1 \tag{10}$$

$$\pi = 0 \qquad \text{on} \quad \xi = \xi_2 \tag{11}$$

Utilizing the boundary conditions on Ψ we may replace Eq. 7 with an equivalent continuity expression of the form

$$\int_{\sigma(\xi)}^{\beta(\xi)} \phi \, d\eta = \lambda \tag{12}$$

It is not difficult to see that the constant λ defined above is a dimensionless residual fluid thickness. The proportionality depends upon the choice of the length scale $\bar{h}$ used in defining η.

Also of interest is the separating force (per unit width transverse to the flow), defined nondimensionally as

$$\Phi \equiv \left(\frac{F}{W}\right)\left(\frac{\bar{h}^2}{\mu U L_x^2}\right) = \int_{\xi_1}^{\xi_2} \pi \, d\xi \tag{13}$$

The goal, then, is to solve Eqs. 4, 5, 12, and 13 for λ and Φ as functions of α, Re, and the shape factors that enter into the

description of the nip region through the specific forms of $\sigma(\xi)$ and $\beta(\xi)$.

So far, the lubrication approximations have not been imposed. Equations 8 and 9 express the no-slip assumption on the kinematics. Boundary conditions on pressure have been the subject of numerous discussions which will not be repeated here.

We select the simplest choice (the Swift-Steiber conditions - Dowson and Taylor, 1979), in Eq. 10 and 11, and we note that the positions ξ_1 and ξ_2 correspond to the ends of the blade (X1 and X2). By its absence from the boundary conditions we see that surface tension effects are assumed to be absent.

An analytical solution to Eqs. 4-6 may be found by a perturbation method. The perturbation parameters are α (accounting for curvature effects) and Re (for inertial effects). Each of the variables is expanded as follows:

$$\begin{pmatrix} \Phi \\ \Psi \\ \Pi \\ \lambda \\ \Phi \end{pmatrix} = \begin{pmatrix} \Phi \\ \Psi \\ \Pi \\ \lambda \\ \Phi \end{pmatrix}^{00} + \alpha \begin{pmatrix} \Phi \\ \Psi \\ \Pi \\ \lambda \\ \Phi \end{pmatrix}^{10} + Re \begin{pmatrix} \Phi \\ \Psi \\ \Pi \\ \lambda \\ \Phi \end{pmatrix}^{01} + \ldots \qquad (14)$$

Variables with superscript (00) give the zeroth-order lubrication approximation. Those with (10) and (01) give the first order corrections for curvature and inertia, respectively.

The Zeroth-Order (Lubrication) Solution

When Eqs. 14 are substituted into Eqs. 4, 5, and 12, and terms in α and Re are dropped, we recover the lubrication equations in the form

$$0 = -\frac{\partial \pi^{00}}{\partial \xi} + \frac{\partial^2 \phi^{00}}{\partial \eta^2} \tag{15}$$

$$0 = -\frac{\partial \pi^{00}}{\partial \eta} \tag{16}$$

$$\int_{\sigma(\xi)}^{\beta(\xi)} \phi^{00}\, d\eta = \lambda^{00} \tag{17}$$

Boundary conditions 8-11 hold, but do not include any constraint on Ψ, which does not appear in this level of approximation.

The solutions may be written as follows:

$$\phi^{00} = \frac{\dot{\pi}^{00}}{2}\eta^2 + \frac{2\phi_0(\xi) - \dot{\pi}^{00}(\sigma^2 - \beta^2)}{2(\sigma - \beta)}\eta + \beta\left(\frac{\dot{\pi}^{00}\sigma}{2} - \phi_0(\xi)\right) \tag{18}$$

where

$$\dot{\pi}^{00} \equiv \frac{\partial \pi^{00}}{\partial \xi} = \frac{12\lambda^{00}}{(\sigma - \beta)^3} + \frac{6\phi_0(\xi)}{(\sigma - \beta)^2} \tag{19}$$

$$\lambda^{00} = \frac{-\int_{\xi_1}^{\xi_2} \frac{\phi_0(\xi)}{(\sigma-\beta)^2}\, d\xi}{2\int_{\xi_1}^{\xi_2} \frac{d\xi}{(\sigma-\beta)^3}} \tag{20}$$

$$\pi^{00}(\xi) = \int_{\xi_1}^{\xi} \left[\frac{12\lambda^{00}}{(\sigma-\beta)^3} + \frac{6\phi_0(\xi)}{(\sigma-\beta)^2}\right] d\xi \tag{21}$$

$$\Phi^{00} = \int_{\xi_1}^{\xi_2} \pi^{00}(\xi)\, d\xi \tag{22}$$

The results are general (to this level of approximation) and can be made particular upon a choice of geometry, $\beta(\xi)$ and $\sigma(\xi)$, and kinematic boundary condition $\phi_0(\xi)$.

Results presented by Hsu indicate that the higher order corrections may not be necessary for our purposes. First order corrections for curvature contributed less that 0.5% to the residual fluid thickness (λ), in the specific case he examined, and the zeroth-order solution was within 1% of a numerically generated solution of the Navier-Stokes equations (Eqs. 1 and 2). First order effects would, however, be important if our primary concernwas for information on blade loading (Φ). Hsu's analysis demonstrated that first order corrections contributed as much as 10% to the dimensionless blade loading. Without attempting to derive the higher order solutions, we examine the results obtained from the zeroth-order approximation, without relying too heavily on the quantitative predictions of blade loading.

The particular choice of geometry and kinematic boundary

condition, as shown in Figure 2, are

Roll Surface $$\sigma'(x) = -\frac{x^2}{2R} \tag{23a}$$

Blade Surface $$\beta'(x) = H - x\,\mathrm{Tan}(\omega) \tag{24a}$$

where $H = \beta'(0) = H_0 - X0\ \mathrm{Tan}(\omega)$

H_0 is the smallest separation (in the y-direction) between the blade and roll.

i.e. $H_0 = \min\{\beta'(x) - \sigma'(x)\} = \beta'(X0) - \sigma'(X0)$

X0 = location of minimum blade separation

i.e. $X0 = \min\{ X2, \max\{ X1, R\sin(\omega)\}\}$

X-Velocity $$u\Big|_{\sigma'(x)} \equiv U_0 = U\left(1 - \frac{x^2}{2R^2}\right) \tag{25a}$$

Y-Velocity $$v\Big|_{\sigma'(x)} = V_0 = -U\left(\frac{x}{R}\right) \tag{26a}$$

In dimensionless form,

$$\sigma(\xi) = -\frac{1}{2}\left(\frac{L_x}{R}\right)\frac{\xi^2}{\alpha^{1/2}} \tag{23b}$$

$$\beta(\xi) = \frac{H}{\bar{h}} - \xi \frac{\tan(\omega)}{\alpha^{1/2}} \tag{24b}$$

$$\Phi_0(\xi) = 1 - \frac{1}{2}\left(\frac{L_x}{R}\right)^2 \xi^2 \tag{25b}$$

$$\Psi_0(\xi) = -\left(\frac{L_x}{R}\right)\frac{\xi}{\alpha^{1/2}} \tag{26b}$$

An obvious choice for the length scales L_x and $\bar{h}$, is

$$L_x = R$$
$$\bar{h} = H$$

where H is the blade height at x=0. However, previous results are presented with $L_x = (R\,\bar{h})^{1/2}$ and for the purpose of comparison is used here as well. The definition of $\bar{h}$ requires a closer look. In addition to $\bar{h}$, three parameters are required to specify the geometry; the blade length, L, blade angle, ω, and the blade displacement, X2. Hsu considered the case of $\omega = 0$ and X2 = 0, for which

$$\beta(\xi) = \frac{H}{\bar{h}}$$

and

$$H = H_0$$

where the obvious choice for $\bar{h}$ is H_0. In this case, H_0 corresponds to the blade height at the downstream edge of the blade (X2) and the minimum separation between the roll and blade.

When X2 = 0 an appropriate choice of reference length , $\bar{h}$, is not obvious. Three possibilities are:

1) Separation between the blade and roll at the downstream edge of the blade.

$$\bar{h} = \beta'(X2) - \sigma'(X2)$$

2) Separation at X = 0.

$$\bar{h} = H$$

3) Minimum separation between blade and roll

$$\bar{h} = H_o$$

For this study, the preferable reference length, $\bar{h}$, is the blade height at X = 0, for X2 $\geq$ 0, and at the downstream edge of the blade for X2 < 0. The downstream edge is chosen when X2 < 0 to avoid negative values of $\bar{h}$. Otherwise, the choice of $\bar{h}$ = H, for X2 $\geq$ 0 , simplifies Eq. 24a nicely. The final expressions defining the geometry and kinematic boundary conditions are:

For X2 $\geq$ 0 :

$$\sigma(\xi) = -\tfrac{1}{2}\xi^2 \tag{23c}$$

$$\beta(\xi) = 1 - \frac{\mathrm{Tan}(\omega)}{\alpha^{1/2}}\xi \tag{24c}$$

$$\phi_o(\xi) = 1 - \tfrac{1}{2}\alpha\xi^2 \tag{25c}$$

$$\Psi_n(\xi) = -\xi \qquad (26c)$$

where

$$\dot{\alpha} = (H/R)$$
$$L_x = (R\,H)^{1/2}$$
$$\bar{h} = H$$

For X2 < 0 :

Equations (23b), (24b),(25b), and (26b) with

$$L_x = (R\,\bar{h})^{1/2}$$
$$\bar{h} = H - X2\,\mathrm{Tan}(\omega) + \frac{X2^2}{2R}$$

RESULTS

Figures 3 and 4 contain justification for considering the zeroth order perturbation solution without higher order contributions for curvature. Hsu's results for λ as a function of H_o/R indicate that first order corrections are small relative to the sensitivity of λ to variations in blade angle and displacement. In the geometry chosen by Hsu, for example, a two degree error in blade angle or 2 mm displacement of the 19 mm blade, results in up to 10% change in λ compared to less than 0.5% for first order curvature effects. This is not to say that first order effects are always insignificant. When blade loading is of primary interest, as it is for Hsu, they are important and should be included. This is shown in Figures 5 and 6 where variations in blade loading associated with curvature effects are comparable to variations due to changes in blade angle and displacement.

The results are very sensitive to blade angle as shown in Figures 3 and 5. It is unlikely, in practice, that the blade angle can be set to within one degree. It is interesting to note that in the limit of zero blade height, the limiting value of λ is 2/3, for a zero degree angle and becomes one for positive blade angles, regardless of how small. Increasing the blade angle increases the residual fluid thickness and decreases the blade loading for a given blade.

Figures 4 and 6 show the effect of blade displacement. The use of blade displacement as a parameter is somewhat artificial because by re-defining the reference frame, displacements can be accounted for by appropriate changes in blade angle. By defining the y-axis as the radius that passes through the downstream edge of the blade, the displacement can be eliminated as a parameter. The reason displacement is considered in this analysis is for the the benefit of providing a sensitivity analysis for an experimental system with a fixed coordinate system, like that used by Hsu and described later in this report. Notice the asymmetry apparent in Figure 6. Displacing the blade upstream (negative x-direction) causes a significant decrease in blade loading, while positive displacements cause less of an effect in the opposite direction. The blade loading has a maximum at X2=L/2 for a zero degree angle, corresponding to the geometry for which the point of tangency of the blade is located at the center of the blade. Positive displacements cause the blade loading to increase until X2=L/2, after which further positive displacement will decrease the blade loading.

Figures 7 and 8 show the effect of blade length on λ and Φ. The range of blade length over which the lubrication theory results are meaningful is limited by two major assumptions. Lubrication theory requires that entrance and exit effects are negligible, $L/H>>1$, and that the blade and roll be nearly parallel to minimize curvature effects, $L/R<<1$. When the blade is large, relative to the roll radius, it extends so far that the curvature of the roll is significant and the parallel flow assumption is violated. At the other extreme, solutions for

small blades are only valid for very small blade heights, because as the blade height increases, the entrance length also increases and entrance effects become significant.

Non-Newtonian Liquids:

Many of the liquids of interest are polymeric solutions or melts which exhibit non-newtonian behavior. We anticipate that the response of such solutions to the wiping process is complicated by non-linear elastic and viscous effects, which can be extremely difficult to model. As a first step in understanding these phenomena, we turn to an analysis of the role of non-linear viscous effects by incorporating a simple shear dependent viscosity function into the analysis.

We begin with the steady two-dimensional dynamic equations in the form

$$\rho\left(u\frac{\partial u}{\partial x}+v\frac{\partial u}{\partial y}\right)=-\frac{\partial p}{\partial x}+\frac{\partial \tau_{xx}}{\partial x}+\frac{\partial \tau_{xy}}{\partial y} \qquad (26)$$

$$\rho\left(u\frac{\partial v}{\partial x}+v\frac{\partial v}{\partial y}\right)=-\frac{\partial p}{\partial y}+\frac{\partial \tau_{xy}}{\partial x}+\frac{\partial \tau_{yy}}{\partial y} \qquad (27)$$

along with the continuity equation

$$\frac{\partial u}{\partial x} + \frac{\partial v}{\partial y} = 0 \tag{28}$$

A useful model for shear viscosity is the power law, a purely viscous (i.e. non-elastic) constitutive equation that we write as

$$\underset{\sim}{\tau} = \mu \underset{\sim}{\Delta} \tag{29}$$

where the rate of deformation tensor has two-dimensional cartesian components

$$\underset{\sim}{\Delta} = \begin{pmatrix} 2\frac{\partial u}{\partial x} & \frac{\partial u}{\partial y} + \frac{\partial v}{\partial x} \\ \frac{\partial u}{\partial y} + \frac{\partial v}{\partial x} & 2\frac{\partial v}{\partial y} \end{pmatrix} \tag{30}$$

The viscosity function is written as

$$\mu = K\left(\tfrac{1}{2}\,\mathrm{II}_{\Delta}\right)^{\frac{n-1}{2}} \tag{31}$$

where

$$\mathrm{II}_{\Delta} = \left(2\frac{\partial u}{\partial x}\right)^2 + 2\left(\frac{\partial u}{\partial y} + \frac{\partial v}{\partial x}\right)^2 + \left(2\frac{\partial v}{\partial y}\right)^2 \tag{32}$$

As in the newtonian case, the variables are nondimensionalized and the dynamic equations display terms to zero and first order in ϵ and Re. The variables are then written as in Eq. 14, and the solutions to various ordersin

and Re may be obtained.

The nondimensionalization is identical to that used in the newtonian case, except that the newtonian viscosity constant of those equations is everywhere replaced by a factor

$$M = K\left(\frac{U}{H_0}\right)^{n-1} \tag{33}$$

We refer to M as the apparent viscosity at the (nominal) shear rate U/H_0.

In dimensionless form, Eq. 31 becomes

$$\bar{\mu} = \frac{\mu}{M} = \left\{2\alpha\left[\left(\frac{\partial\phi}{\partial\xi}\right)^2+\left(\frac{\partial\psi}{\partial\eta}\right)^2\right]+\left(\frac{\partial\phi}{\partial\eta}+\alpha\frac{\partial\psi}{\partial\xi}\right)^2\right\}^{\frac{n-1}{2}} \tag{34}$$

and $\bar{\mu}$ itself is included in the perturbation expansion in the form

$$\bar{\mu} = \bar{\mu}^{00} + \alpha\bar{\mu}^{10} + Re\,\bar{\mu}^{01} + \ldots \tag{35}$$

As in the newtonian case, we concern ourselves only with the zeroth order solution, but for different reasons. Although the power law constitutive equation is a useful mathematical model for investigating the effect of a shear dependent viscosity, it is not expected to model quantitatively the behavior of any "real" fluid involved in the wiping process. An immense amount of algebra is required to generate the first order contributions, and it is more reasonable to extract information from the zeroth order solution and compare that to the behavior of some real fluids.

The Zeroth Order Solution:

The equations are (Cf: Eqs. 15-17)

$$0 = -\frac{\partial \Pi^{oo}}{\partial \xi} + \frac{\partial}{\partial \eta}\left[\bar{\mu}^{oo}\left(\frac{\partial \phi^{oo}}{\partial \eta}\right)\right] \tag{36}$$

$$0 = -\frac{\partial \Pi^{oo}}{\partial \eta} \tag{37}$$

$$\int_{\sigma(\xi)}^{\beta(\xi)} \phi^{oo}\, d\eta = \lambda^{oo} \tag{38}$$

where

$$\bar{\mu}^{oo} = \left[\left(\frac{\partial \phi^{oo}}{\partial \eta}\right)^2\right]^{\frac{n-1}{2}} \tag{39}$$

Boundary conditions 8-11 hold.

Unfortunately, no analytical solution of these equations may be found. Instead, we adopt a procedure due to Horowitz and Steidler (1960) and produce numerical solutions for the variables of interest.

One advantage of the Horowitz/Steidler procedure is that it can be generalized to any purely viscous constitutive equation. We rewrite Eq. 36 as

$$0 = -\frac{\partial \Pi^{oo}}{\partial \xi} + \frac{\partial \tau^{oo}}{\partial \eta} \tag{40}$$

where

$$\tau^{oo} = \bar{\mu}^{oo} \frac{\partial \phi^{oo}}{\partial \eta} \tag{41}$$

but $\bar{\mu}^{oo}$ is left unspecified at this stage. We define a function $f(\tau^{oo})$ as

$$f(\tau^{oo}) = \frac{\partial \phi^{oo}}{\partial \eta} \tag{42}$$

(in the following, we drop all superscripts that denote the zeroth-order solution.)

Integration of Eq. 40 yields

$$\tau = \eta \dot{\Pi} + \tau_\beta \tag{43}$$

where $\tau_\beta = \tau \Big|_{\eta = \beta(\xi)}$

Integration of Eq. 42 using Eq. 9 gives

$$\phi = \int_{\sigma(\xi)}^{\eta} f(\tau)\, d\eta + \phi_0(\xi) \tag{44}$$

Using Eq. 43, we write this as

$$\phi = \frac{1}{\dot{\Pi}} \int_{\tau_\sigma}^{\tau} f(\tau)\, d\tau + \phi_0(\xi) \tag{45}$$

With the boundary condition $\phi = 0$ at $\eta = \beta(\xi)$ we may write this

as

$$\dot{\Pi} = \frac{-1}{\phi_0(\xi)} \int_{\tau_\sigma}^{\tau_\beta} f(\tau)\, d\tau = \left[F(\tau_\sigma) - F(\tau_\beta)\right] \frac{1}{\phi_0(\xi)} \tag{46}$$

where we define

$$F(\tau) \equiv \int_0^{\tau} f(\tau)\, d\tau \tag{47}$$

With these results we may write λ in the form

$$\lambda = \int_\sigma^\beta \phi\, d\eta = \frac{1}{\dot{\Pi}^2} \int_{\tau_\sigma}^{\tau_\beta} \left[F(\tau) - F(\tau_\sigma)\right] d\tau + \int_{\tau_\sigma}^{\tau_\beta} \phi_0 \frac{d\tau}{\dot{\Pi}}$$

$$= \frac{1}{\dot{\Pi}^2} \left[G(\tau_\beta) - G(\tau_\sigma) - (\tau_\beta - \tau_\sigma) F(\tau_\sigma)\right] + \frac{\phi_0}{\dot{\Pi}} (\tau_\beta - \tau_\sigma) \tag{48}$$

where

$$G(\tau) \equiv \int_0^{\tau} F(\tau)\, d\tau \tag{49}$$

From Eq. 43 we write

$$\dot{\Pi} = \frac{\tau_\beta - \tau_\sigma}{(\beta - \sigma)} \tag{50}$$

If we regard τ_β, τ_σ, λ, and Π as the unknowns, we may use Eqs. 46, 48, and 50 in an iterative approach as follows:

1) A constitutive equation is selected, so that $f(\tau)$ is given as an explicit function. Hence the integrals F and G may be obtained.

2) A trial value for λ is assumed.

3) Regarding τ_β, τ_σ, and $\dot{\Pi}$ as the unknowns at each position ξ, we assume a ξ value, calculate $\sigma(\xi)$, $\rho(\xi)$, and ϕ_0 and solve for τ_β, τ_σ, and $\dot{\Pi}$ at each ξ on the range $\xi_1 < \xi < \xi_2$.

4) From $\dot{\Pi}$ and the boundary condition $\Pi = 0$ at $\xi = \xi_1$ we integrate to obtain the function $\Pi(\xi)$. If $\Pi(\xi_2)$ does not satisfy the boundary condition $\Pi = 0$ at $\xi = \xi_2$, we change λ and carry out another calculation of $\Pi(\xi)$, until satisfactory convergence is attained.

This method is checked by carrying out the procedure for a newtonian fluid, for which an analytical solution for $\Pi(\xi)$ and λ is available (through the zeroth-order newtonian analysis presented earlier). Satisfactory results are obtained, as shown in Figures 9a and 9b.

RESULTS

For a power law fluid, for which

$$f(\tau) = |\tau|^{\frac{1}{n}-1}\tau \tag{51}$$

$$F(\tau) = \frac{1}{q}|\tau|^{q} \qquad \left(q = \frac{1}{n}+1\right) \tag{52}$$

$$G(\tau) = \frac{1}{q+1}\tau F(\tau) \tag{53}$$

one obtains the results shown in Figures 10-17 (See Table 2 for Key to Figures 10-17). $\Phi^{\circ\circ}$ is calculated as before (i.e.using Eq. 13), but for a power law fluid

$$\Phi^{\circ\circ} = \left(\frac{F}{W}\right)\left(\frac{H}{MUR}\right) \tag{54}$$

with M, the apparent viscosity, calculated from Eq. 33. We note that U/H_o is an arbitrary but useful definition of a characteristic shear rate in this geometry.

Figures 10-12 and 14-16 show that the residual fluid thickness increases as the liquid becomes increasingly shear thinning (i.e. as n decreases) and is relatively unaffected by

small changes in blade angle or displacement. The increase is small and shows a slight dependence on H/R.

Figures 13 and 17 show the effect of shear thinning on blade loading with blade angle and displacement as parameters, respectively. Blade height is predicted to have a significant effect, but small changes in angle and displacement do not.

EXPERIMENTAL

Apparatus:

Figure 18 shows a sketch of the wiping apparatus. A cylindrical steel roll is half immersed in the test fluid and driven at constant speed, U. Liquid is entrained by the moving roll and is partially wiped by the blade, while the remainder emerges downstream as residual fluid of thickness, h. The blade is held in a rig which permits accurate positioning of the blade relative to the roll.

The roll has a radius of 2.75 inches, accurately machined to within 0.5 mil, and an axial length of 5 inches. Blades made from aluminum are interchangeable and have the geometry defined in Figure 19. Table 2 summarizes the specific geometries discussed in this report.

Residual fluid thickness is measured by a direct contact method (Greener, 1978) using a micrometer driven needle positioned 60 degrees downstream of the blade. The contact of the needle with the surface is observed through a microscope.

Procedure:

It is unfortunate that in the limit of very small blade height ($H_o \rightarrow 0$), when the lubrication approximations are most likely to be valid, good experimental data are very difficult to obtain. Because of unavoidable experimental uncertainty and the

finite precision with which the roll is machined, there is always some error associated with measuring both the blade height, H_e, and residual fluid thickness, h. The small but finite uncertainties amount to large relative errors in residual fluid thickness as $H_e \rightarrow 0$. If the blade height and the corresponding residual fluid thickness are accurately known at one setting, however, precise incremental changes can be made. A procedure for gathering and presenting data is adopted, which minimizes the experimental uncertainty by taking advantage of the precision involved in measuring increments in H_e and h.

Blade height is arbitrarily set to a large value (greater than 50 mil) and the corresponding residual fluid thickness is measured. The blade height is then incrementally decreased, with the associated micrometer reading for residual fluid thickness recorded for each increment, until the blade touches the roll (corresponding to $H_e = 0$). The roll is then stopped and the needle is lowered until it too touches the roll, and the micrometer reading is recorded (corresponding to $h = 0$). The data generate a curve of h as a function of H_e. This curve as a whole can then be shifted, within bounds set by the experimental uncertainty (a maximum of 1 mil in any direction), so that it passes smoothly through the origin. In this way, the errors involved in individual data points are averaged out over the entire curve.

RESULTS

The range over which certain experimental variables are considered is determined by experimental limitations. In order to flood the inlet (upstream) region of the blade, a sufficient quantity of fluid must be entrained from the reservoir as shown in Figure 2a. The amount entrained depends upon both the roll speed and the fluid properties (Campanella, 1984). For a given fluid, the roll speed is limited on the low end by this flooding criterion. On the high end, there is also a limit, corresponding to the onset of instabilities and/or air entrainment . Under unstable wiping conditions, the residual fluid layer is no longer smooth and often develops a "ribbed" pattern (Pearson, 1960, Sullivan, 1979) transverse to the direction of flow. Positive blade placements and negative blade angles are found to promote this instability. When stability is not a problem, there is a limit on roll speed above which air is entrained into the test fluid at the interface where the roll surface re-enters the bath (Burley, 1984). The range of roll speeds investigated is from 2 to 20 in/sec, depending on the test fluid. To obtain flooding of the blade, a lower limit on the viscosity of newtonian test fluids is about 3 poise.

Two newtonian liquids are examined: glycerine and Karo syrup. Under conditions that the blade inlet is flooded, no effect of linear roll speed on residual fluid thickness is observed. Figure 20 shows data for glycerine and Karo syrup with a 1/4 in. blade at 0 degrees and the corresponding results

predicted by lubrication theory. Results for glycerine and Karo syrup are identical (within experimental uncertainty) even though their viscosities differ by almost an order of magnitude. In other geometries, similar agreement between the two is found. The remainder of the newtonian results presented are for glycerine, with the assumption that they are representative of newtonian liquids in general.

In Figure 20, agreement between the data and lubrication theory is good for small blade heights , but becomes poor as H_o increases, while in Figure 21, the data and theory are in good agreement up to the maximum blade height shown (50 mils). The poor agreement with small blades at large blade heights is due to entrance effects not accounted for by lubrication theory. When H_o = 50 mils, L/H_o = 10 for the 1/2 in. blade, but only 5 for the 1/4 in. blade. Data indicate that $L/H_o > 10$ is a reasonable estimate of the requirement that entrance effects are negligible. Notice that when entrance effects are significant, data lie above the theory as expected on the basis of momentum transfer arguments (Appendix A). Blades larger than 1/2 in. are not used for two reasons. With the 1/2 in. blade and 2.75 in. radius roll, L/R = 0.18. Larger blades would likely invalidate the negligible curvature assumption, $L/R << 1$, and at the same time require a large amount of fluid to flood the inlet region of the blade. This flooding problem (see Figure 2a), limits the blade geometry in a number of cases.

Changing the blade angle from zero to 10 degrees affects the residual fluid thickness as shown in Figures 22, 23, and 24, for three blade lengths. Surprisingly good agreement between

experimental data and simple lubrication theory is found for the 1/2 in. blade. Note that as the blade size decreases, the data fall further above lubrication theory predictions due to entrance effects. Blade angles larger than 10 degrees are not discussed because of large curvature effects and the problem of flooding the inlet region of the blade. Some experiments performed with large blade angles (e.g. 45 degrees) produced data that fell below lubrication theory predictions, but it is unknown whether this effect was due to curvature or an inadequately flooded inlet region.

Figures 25 and 26 show the effect of blade displacement and are also good examples of the above mentioned flooding problem. Once again, data for the largest blade (L=1/2 in) are in good agreement with theory, but only for three of the four displacements shown. The data for the largest negative displacement (X2=-0.5) fall below the theory. This is a prime example of not enough fluid being entrained by the roll to flood the inlet region of the blade. The problem is exacerbated when the blade angle is increased, as shown in Figure 26.

Non-Newtonian Liquids:

Predicting the behavior of viscoelastic liquids is difficult in even the simplest flow problems and is complicated further by the converging-diverging nature of the wiping process. We do not expect good quantitative agreement between the simple power law

lubrication theory model and residual fluid thickness data for real viscoelastic fluids, but rather hope to gain insight into the effect the shear dependent viscosity has on the results.

Figure 27 shows viscometric data, taken with a Rheometrics Fluids Rheometer, for a shear thinning carboxymethylcellulose (CMC) solution. For a linear roll speed of 10 in/sec and blade heights ranging from 10 to 50 mils, the nominal shear rate ranges from 200 to 1000 1/sec. In this range the power law index, n, is about 0.6. Note, however, that the fluid also exhibits a finite normal stress. At a representative shear rate of 500 1/sec, the recoverable shear, S_R, defined by

$$S_R = \frac{N1\ \dot{\gamma}^2}{2\tau_{12}} \tag{55}$$

where

$$N1 = \frac{\tau_{11} - \tau_{22}}{\dot{\gamma}^2}$$

and

$$\dot{\gamma} = \text{shear rate}$$

is also about 0.6. The recoverable shear is a parameter commonly used to estimate the relative importance of elastic and viscous effects. When we examine data for the CMC solution, we observe the results of both shear thinning and elastic effects, while the power law lubrication theory only accounts for the shear thinning behavior.

Figure 28 shows that the residual fluid thickness of the CMC solution is considerably greater than that for glycerine and is also greater than predicted by lubrication theory. Since shear thinning behavior is accounted for in the model, it is reasonable

to suspect that the increase in thickness is due to elastic effects. To test this hypothesis, small amounts of high molecular weight polyacrylamide (PAM) are added to the CMC solution, to increase the recoverable shear without significantly affecting the power law index. Data for two such solutions are included in Figure 28, one with a recoverable shear of 0.9 and the other with 1.4. Note that by increasing the recoverable shear, the residual fluid thickness decreases rather than increases. The data for the solution with the largest recoverable shear fall below those of the newtonian fluid. This is opposite to the effect predicted by the power law lubrication theory model.

In an attempt to isolate elastic and shear thinning effects, the behavior of an elastic fluid with insignificant shear thinning (i.e., a Boger fluid - Boger, 1977) is examined. The fluid is made by adding a small amount of high molecular weight PAM to corn syrup. Figures 29 and 30 show viscometric data for the Boger fluid as well as for a CMC solution and glycerine. Note that the viscosity of the Boger fluid is nearly constant over the shear rate range for which data were collected. The Boger Fluid also exhibits large normal stresses in steady shear relative to the highly shear thinning (n=0.6) CMC solution.

Figure 31 shows a drastic decrease in residual fluid thickness with the Boger fluid relative to glycerine. Note that although the CMC data fall above the power law lubrication theory curve, it is in better agreement for the larger 1/2 in. blade than for either the 1/4 in. blade (Figure 32) or the 0.068 in. blade (Figure 33). This is attributed to entrance effects, which

for flow in pipes are known to be considerably longer for viscoelastic fluids than those encountered with newtonian fluids (Tung, 1978). Results in Figures 31-33 demonstrate that the elastic solution exhibits a greatly decreased residual fluid thickness in comparison to lubrication theory models. The amount of viscoelastic fluid left behind after the wiping process appears to depend on the competing effects of shear thinning, causing it to increase, and elasticity, causing it to decrease.

CONCLUSIONS

Experimental results for newtonian liquids are very useful for determining the range of validity of the lubrication theory model, but unfortunately, that range is severely limited. One obvious inadequacy of the model is the negligible curvature assumption, which is only valid for very small wiper angles. Another is the assumption of negligible entrance effects, which appears to be violated for thin wipers. The model also fails to take into account surface tension effects by using the Swift-Steiber boundary conditions. A useful estimate of the magnitude of surface tension effects is the dimensionless capillary number defined by

$$N_{Ca} = \frac{\mu U}{\sigma^*} \tag{56}$$

The fact that N_{Ca} is of order unity in some of our experiments indicates that surface tension may be significant. Gravitational effects are neglected in the model as well, and can be estimated by another dimensionless group, the Stokes parameter, defined by

$$St = \frac{\rho g H_0^2}{\mu U} \tag{57}$$

If the blade height is large and the roll speed is low, St can be as large as 0.2, but in most of our experiments gravitational effects are negligible. (Note: Centrifugal effects are always

negligible). Obviously, a less restrictive model of the wiping process is required, but since an analytical solution is very unlikely, it is necessary to consider the use of numerical techniques.

We are presently attempting to use the Finite Element Method (FEM) to solve the blade wiping problem for newtonian fluids without the simplifying assumptions mentioned above. Surface tension, which is neglected by the use of the Swift-Steiber boundary conditions in the lubrication theory model, can be accounted for by treating the region downstream of the blade as a free surface problem. The effects of gravity, inertia, and curvature are relatively easy to incorporate into the numerical scheme as well, so that the rigid blade wiping problem can be completely solved for newtonian liquids.

Even with sophisticated numerical techniques, it is unlikely that the wiping problem can be solved in general for viscoelastic liquids. With newtonian liquids, the formulation of the problem is straightforward because of the simple and predictable manner in which they respond to imposed deformations. Viscoelastic liquids, on the other hand, exhibit extremely complex behavior which is dependent on both the magnitude and duration of deformation imposed. Unlike the newtonian case, a constitutive equation does not exist that is capable of describing viscoelastic fluid behavior in a general flow field. Nonlinear viscous behavior alone, is relatively easy to model, the power law fluid being a simple example. The difficulties arise because the viscous effects are coupled with transient and deformation history dependent behavior associated with the "elasticity" of

the fluid. Today, flow problems are solved using constitutive equations chosen according to a compromise between algabraic tractability and physical reality. Such equations are highly dependent on the nature of the flow field and are limited to special classes of problems. The wiping problem is a formidible problem for a constitutive equation to model because fluid particles experience rapidly changing deformations in time, which can be of considerable importance for viscoelastic fluids (Shirodkar, 1982). Elastic liquids can exhibit large transient shear stresses as well as extensional stresses when undergoing the rapid changes in deformation rate that are present because of the converging nature of the flow. The reulting kinematics for viscoelastic liquids are often drastically different from those present for newtonian liquids (Doremus, 1983, Mensah, 1984, Metzner, (1969).

Key to solving the problem of modeling viscoelastic fluid behavior is determing which material properties are most responsible for the behavior of a given fluid in a particular flow field. We have mentioned the recoverable shear, which is a steady viscometric material property providing a measure of the relative importance of elastic and viscous effects in steady shear flow. An important question is, can material properties measured in steady viscometric flows provide insight into how an elastic liquid will behave in a transient flow field? If not, what are the pertinent transient fluid properties to measure and how can they be incorporated into useable and realistic constitutive equations?

Given the difficulty involved in choosing an appropriate constitutive equation to model the wiping process, it is fortunate that we are able to use experimental data to evaluate proposed constitutive equations. Finding a constitutive equation to best fit the data is equivalent to determining which material properties of the fluid dominate the flow field. As a simple example, if the power-law model had fit the data nicely, we would conclude that the shear thinning nature of the fluid is most responsible for the resulting behavior. In fact, such is the case for the CMC solution with the lowest recoverable shear. There is an increase in λ over newtonian values as predicted by the model, although a little more dramatic than expected. However, as the elasticity of the fluid is increased by the addition of polyacrylamide, as reflected in an increased recoverable shear, the trend in λ is reversed. The shear dependent viscosity is obscured by another fluid property associated with the elasticity of the fluid. The data provide experimental evidence of this fact, and is a good test for evaluating constitutive equations to be used to model the process. In this way we can obtain a better understanding of the important features of the wiping process.

This study provides a good foundation for understanding the rigid blade wiping process, but equally important, it provides some insight into a direction for future work. A Finite Element solution to the newtonian problem is required to understand the effects of inertia and surface tension and explore thin wipers and large wiper angle geometries. With the newtonian problem well understood, experimental data for well characterized viscoelastic fluids can be compared to newtonian results and provide

information regarding more quantitative aspects of non-newtonian and elastic effects. An obvious extension of the rigid blade wiping problem is to the study of wiping with flexible blades. This problem is much more complicated than the rigid wiper case because the geometry is unknown a-priori and depends upon the complex interaction of hydrodynamic forces and wiper properties (Saita, 1984). Fortunately, the solution to the rigid wiper problem provides the logical first step in understanding the influence of geometry on the hydrodynamic forces that develop under a wiper and is a valuable tool for further study.

VARIABLES

F/W - force per unit width on blade

h - residual fluid thickness

$\bar{h}$ - characteristic length in the y-direction

H - blade height at x=0

H_o - minimum clearance between the blade and the roll

K - parameter in power-law fluid model

L - blade length

L_e - entrance length (Appendix A)

L_x - characteristic length in x-direction

n - power-law index

N1 - primary normal stress coefficient (page 30)

P - pressure

Q - flow rate

R - roll radius

Re - Reynolds number (page 5)

U - linear roll speed

u - velocity in x-direction

$u_o(x)$ - u-velocity on roll surface

v - velocity in y-direction

$v_o(x)$ - v-velocity on roll surface

x - space coordinate in the primary flow direction

X0 - x-coordinate at the point of minimum blade clearance

X1 - x-coordinate at the upstream edge of the blade

X2 - x-coordinate at the downstream edge of blade

y - space coordinate transverse to primary flow direction

Variables: (page 2)

α - geometric parameter (page 5)

$\beta'(x)$ - function describing the blade surface (linear)

$\beta(\xi)$ - dimensionless blade surface

$\delta(x)$ - boundary layer thickness (Appendix A)

$\underset{\sim}{\Delta}$ - rate of deformation tensor

η - dimensionless space coordinate - $y/\bar{h}$ (page 4)

λ - dimensionless residual fluid thickness - $h/\bar{h}$ (page 6)

μ - viscosity

ξ - dimensionless space coordinate - x/L_x (page 4)

π - dimensionless pressure (page 4)

Π_A - second invariant of $\underset{\sim}{\Delta}$

ρ - density

$\sigma'(x)$ - function describing the roll surface (quadratic)

$\sigma(\xi)$ - dimensionless roll surface

σ^* - surface tension

$\underset{\sim}{\tau}$ - stress tensor

τ_{ij} - i,j component of the stress tensor

ϕ - dimensionless u-velocity (page 4)

$\phi_o(\xi)$ - dimensionless $u_o(x)$ (page 11)

$\bar{\Phi}$ - dimensionless blade loading (page 13)

Ψ - dimensionless v-velocity (page 4)

$\Psi_o(\xi)$ - dimensionless $v_o(x)$ (page 11)

ω - blade angle

Symbol	Ho/R	Angle (deg) or Displacement (mm)
○	0.006	0
●	0.015	0
◑	0.025	0
△	0.006	+ 1
▲	0.015	+ 1
◭	0.025	+ 1
□	0.006	- 1
■	0.015	- 1
◨	0.025	- 1

TABLE 1: Key to Figures 10-17

Blade Length (L)	Blade Angle (ω)
0.5 in.	0 deg. 10 deg.
0.25 in.	0 deg. 10 deg.
0.068 in.	0 deg. 10 deg.

TABLE 2: Blade Geometries

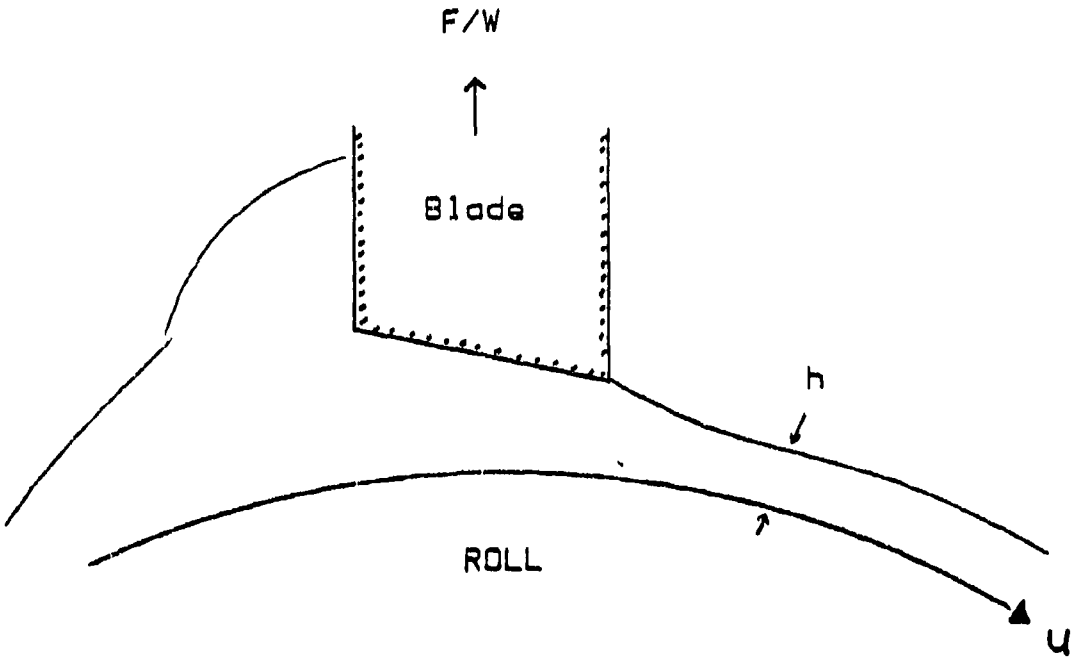

FIGURE 1: Configuration of a simple Blade-Over-Roll Wiper

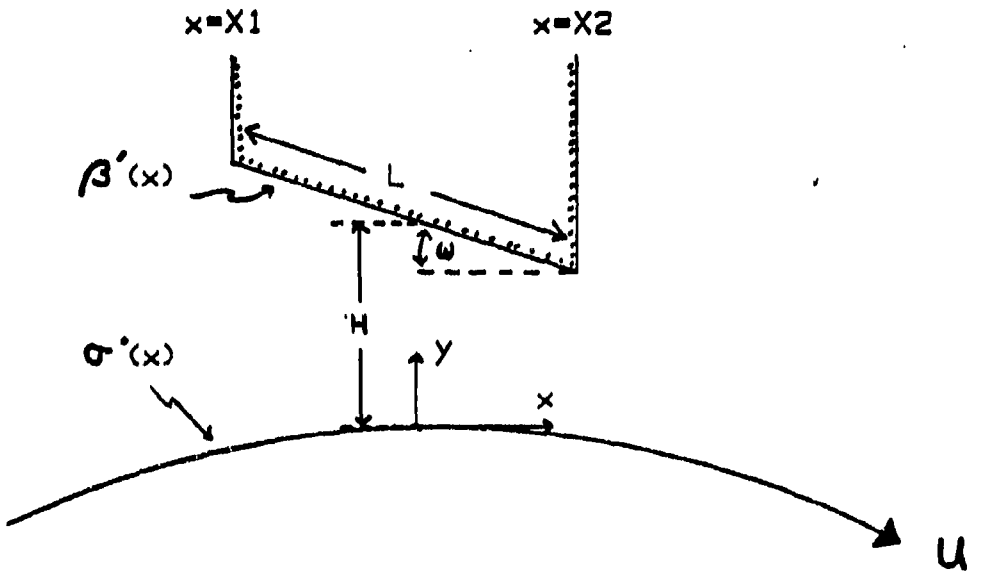

FIGURE 2: Definition sketch of the Geometry

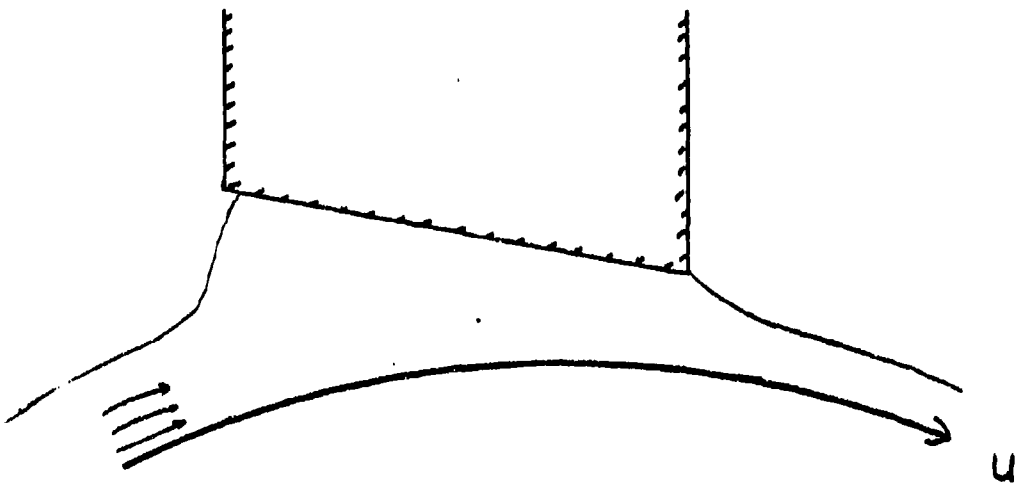

Figure 2a: Schematic showing an example of the "FLOODING PROBLEM". The inlet region of the blade is not supplied with an adequate amount of fluid from the bath.

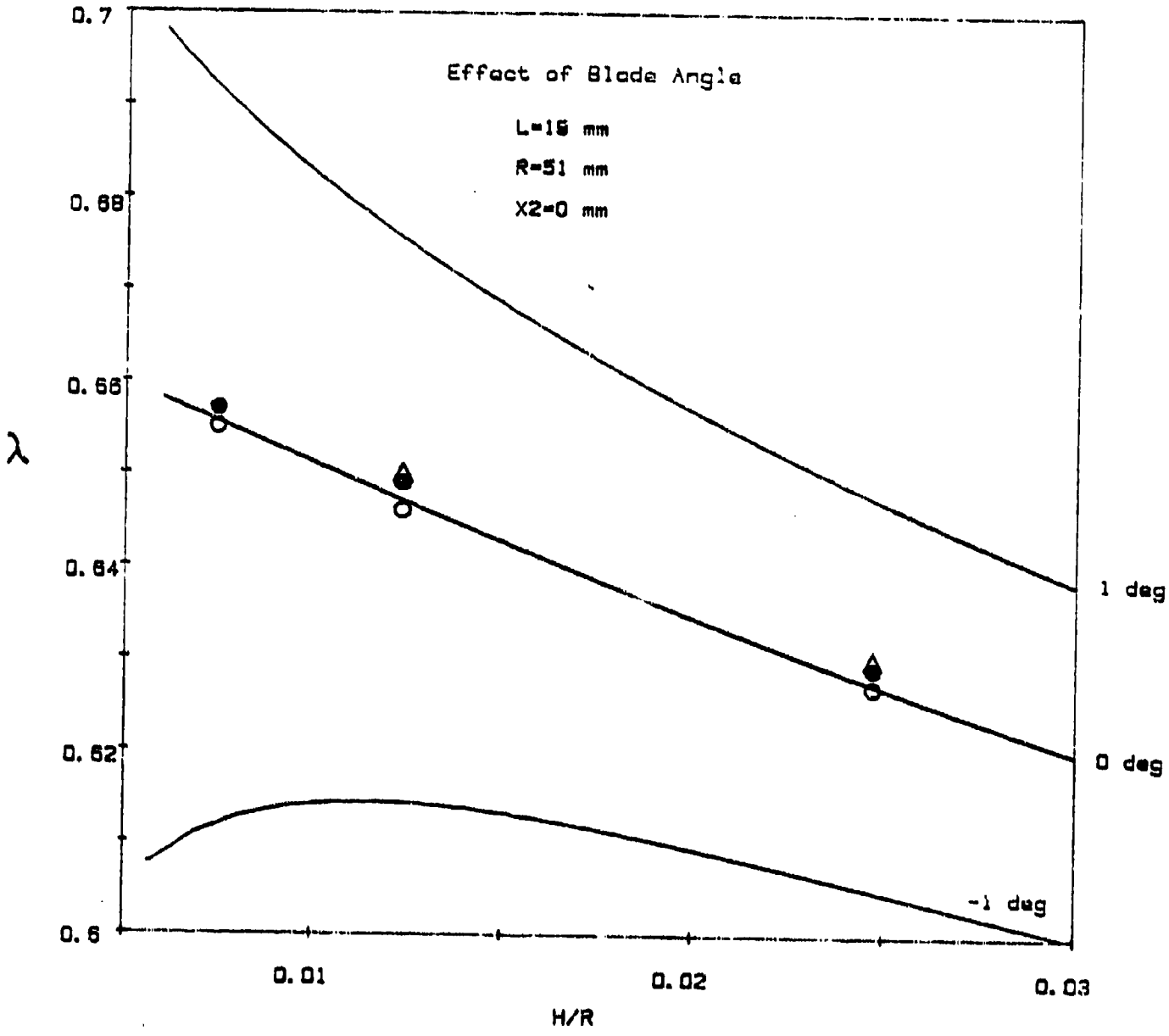

FIGURE 3: Effect of blade angle on Residual Fluid Thickness (λ). Solid lines are Lubrication Theory for a Newtonian liquid. Symbols are from Hsu (1984)

- ○ - Zeroth order solution
- ● - First order curvature included
- △ - Finite Element Solution

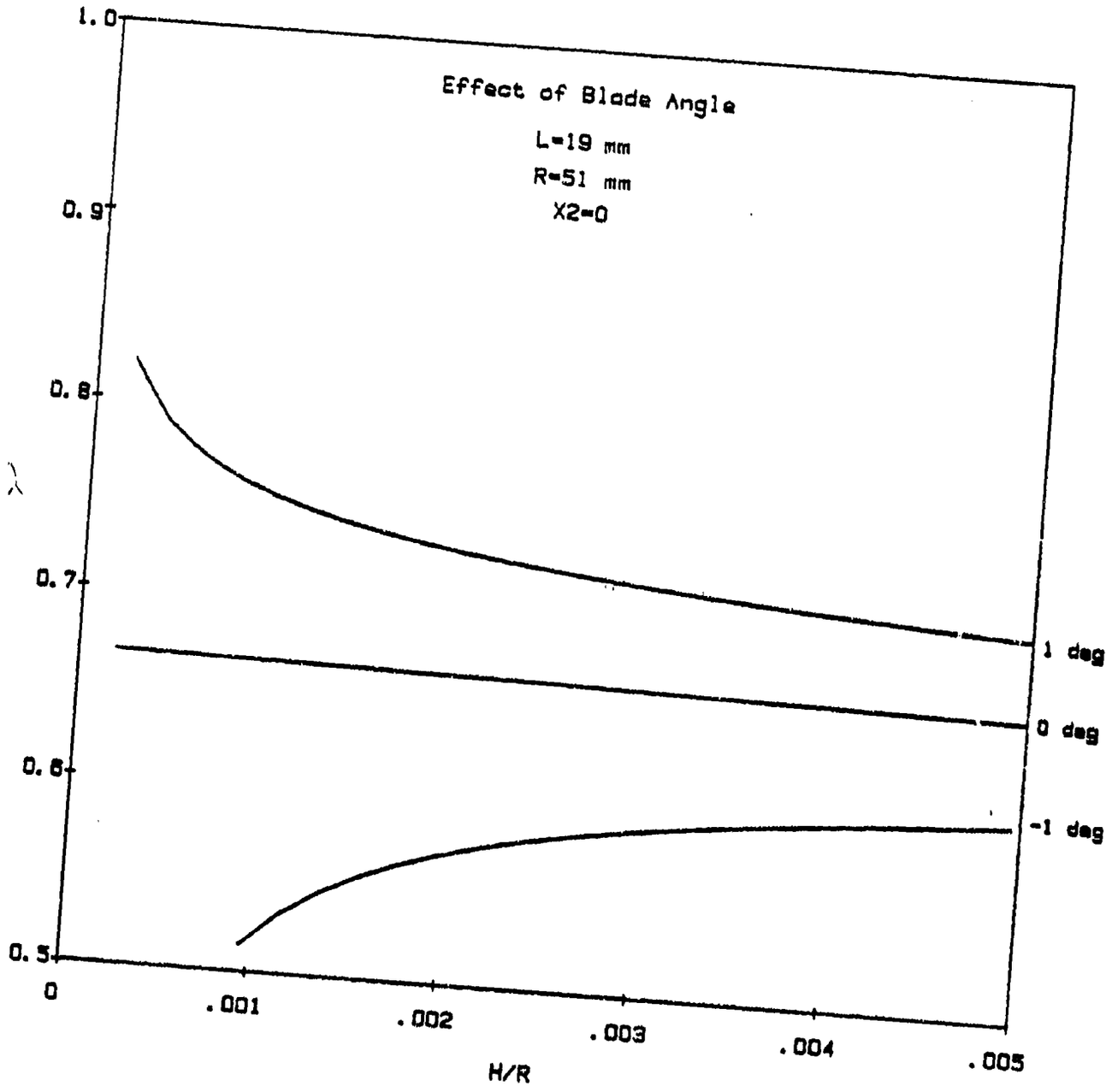

FIGURE 3a: Effect of blade angle on Residual Fluid Thickness (λ). Solid lines are Lubrication Theory for a Newtonian liquid.

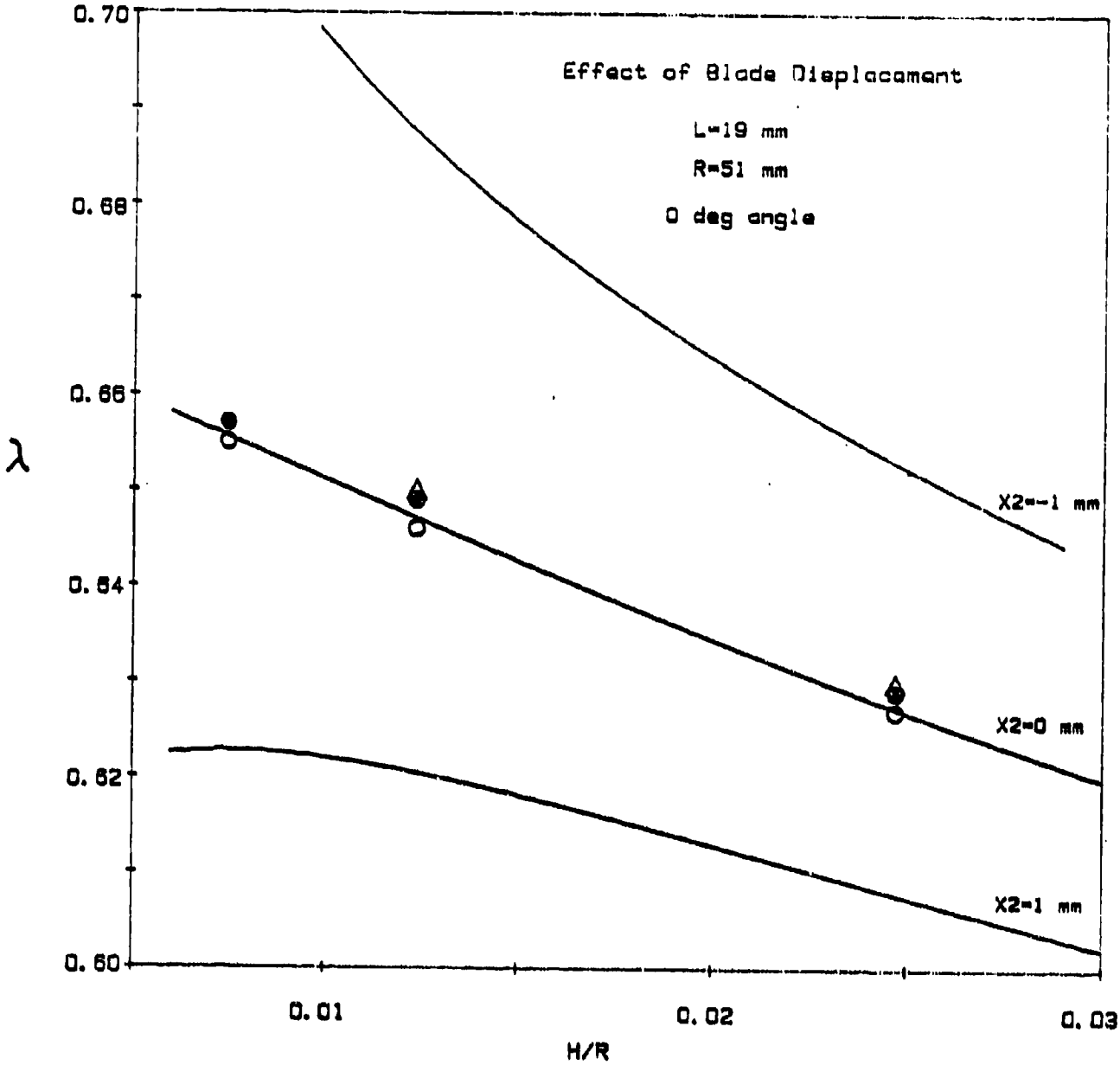

FIGURE 4: Effect of blade displacement on Residual Fluid Thickness (λ). Solid lines are Lubrication Theory for a Newtonian liquid. Symbols are from Hsu (1984).
- ○ - Zeroth order solution
- ● - First order curvature included
- △ - Finite Element Solution

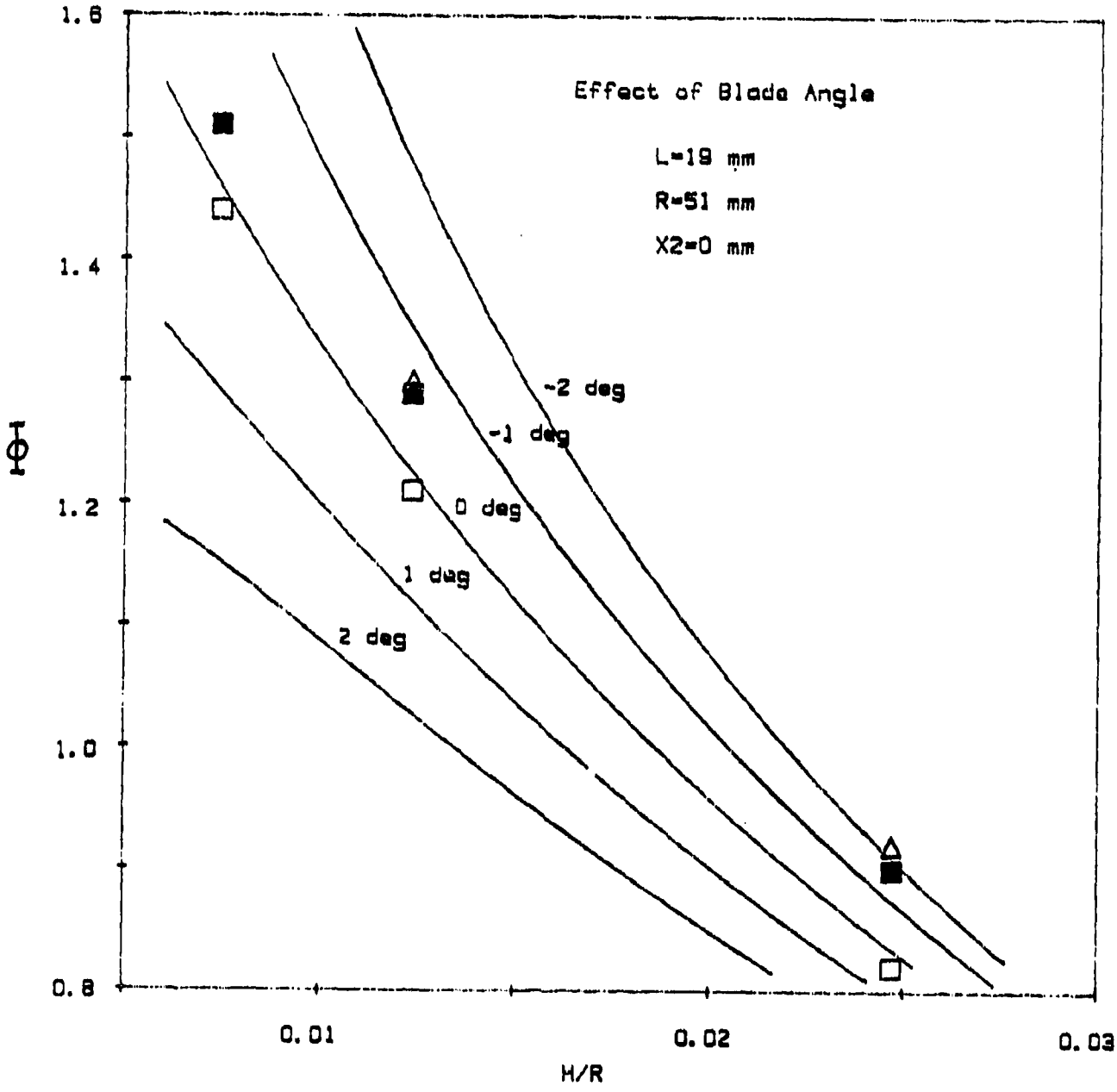

FIGURE 5: Effect of blade angle on Blade Loading. Solid lines are Lubrication Theory for a Newtonian liquid. Symbols are from Hsu (1984).

□ - Zeroth order solution

■ - First order curvature included

△ - Finite Element Solution

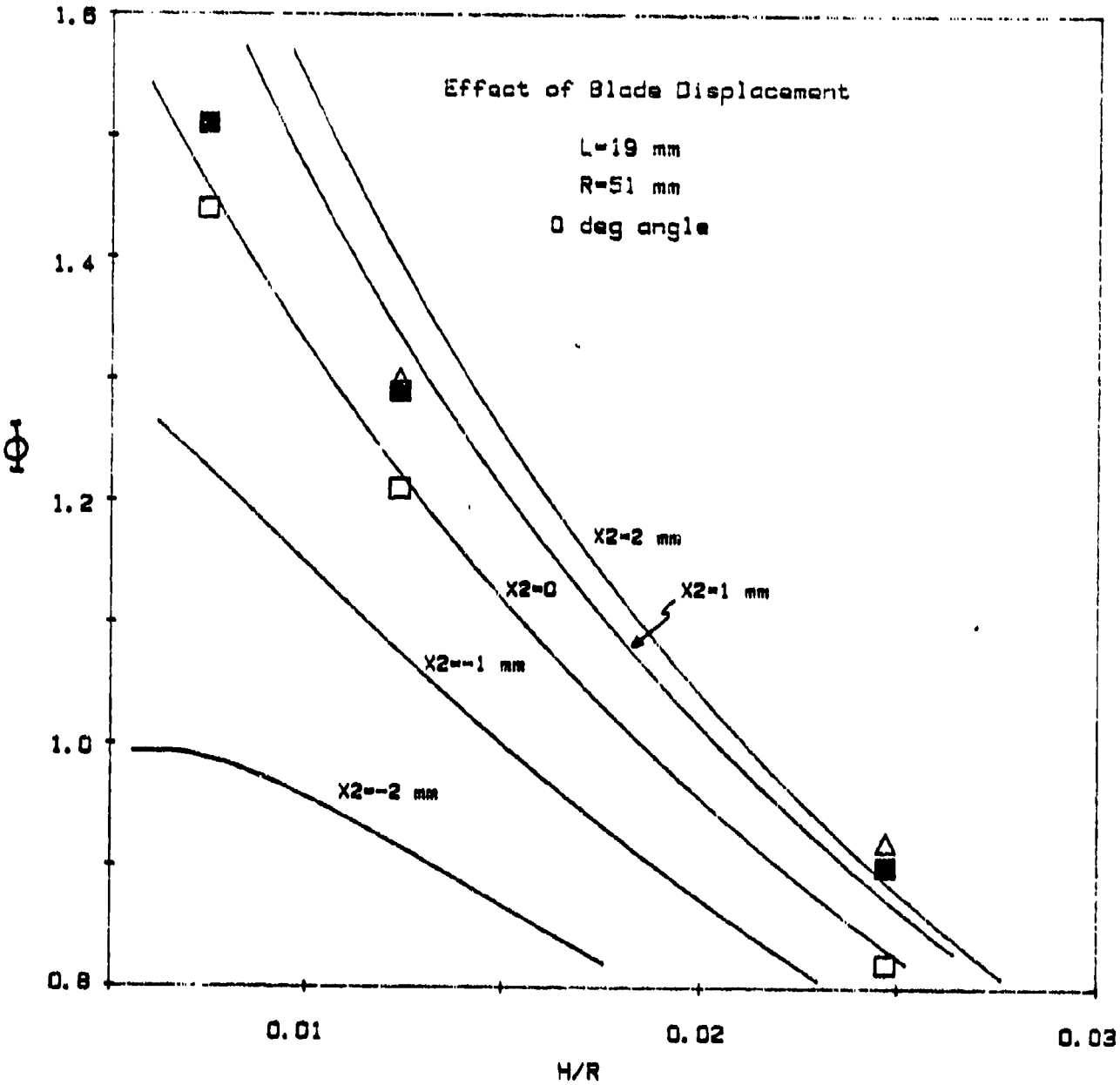

FIGURE 6: Effect of blade displacement on Blade Loading. Solid lines are Lubrication Theory for a Newtonian liquid. Symbols are from Hsu (1984).
□ - Zeroth order solution
■ - First order curvature included
△ - Finite Element Solution

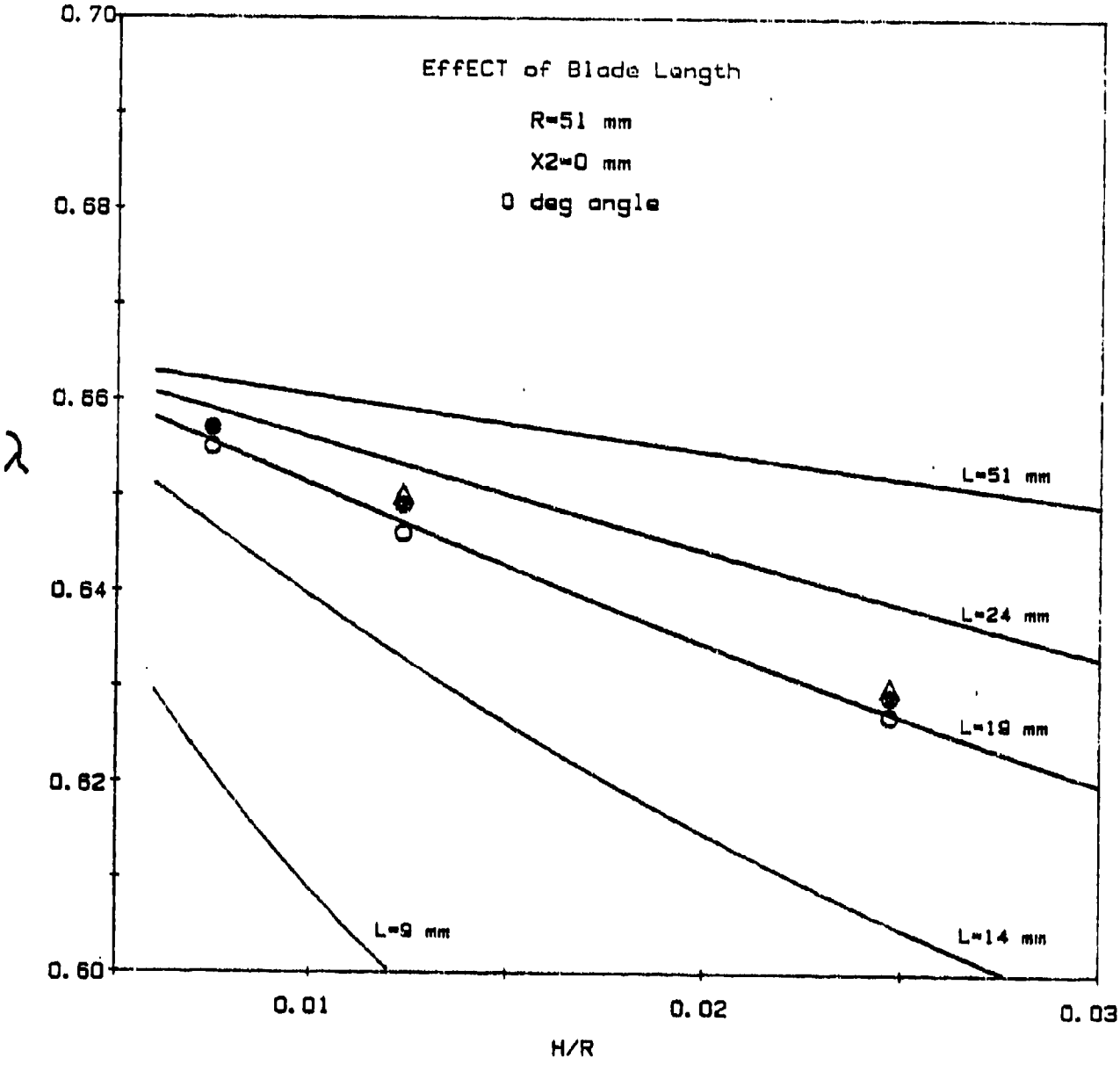

FIGURE 7: Effect of blade length on Residual Fluid Thickness (λ). Solid lines are Lubrication Theory for a Newtonian liquid. Symbols are from Hsu (1984).

- ○ - Zeroth order solution
- ● - First order curvature included
- △ - Finite Element Solution

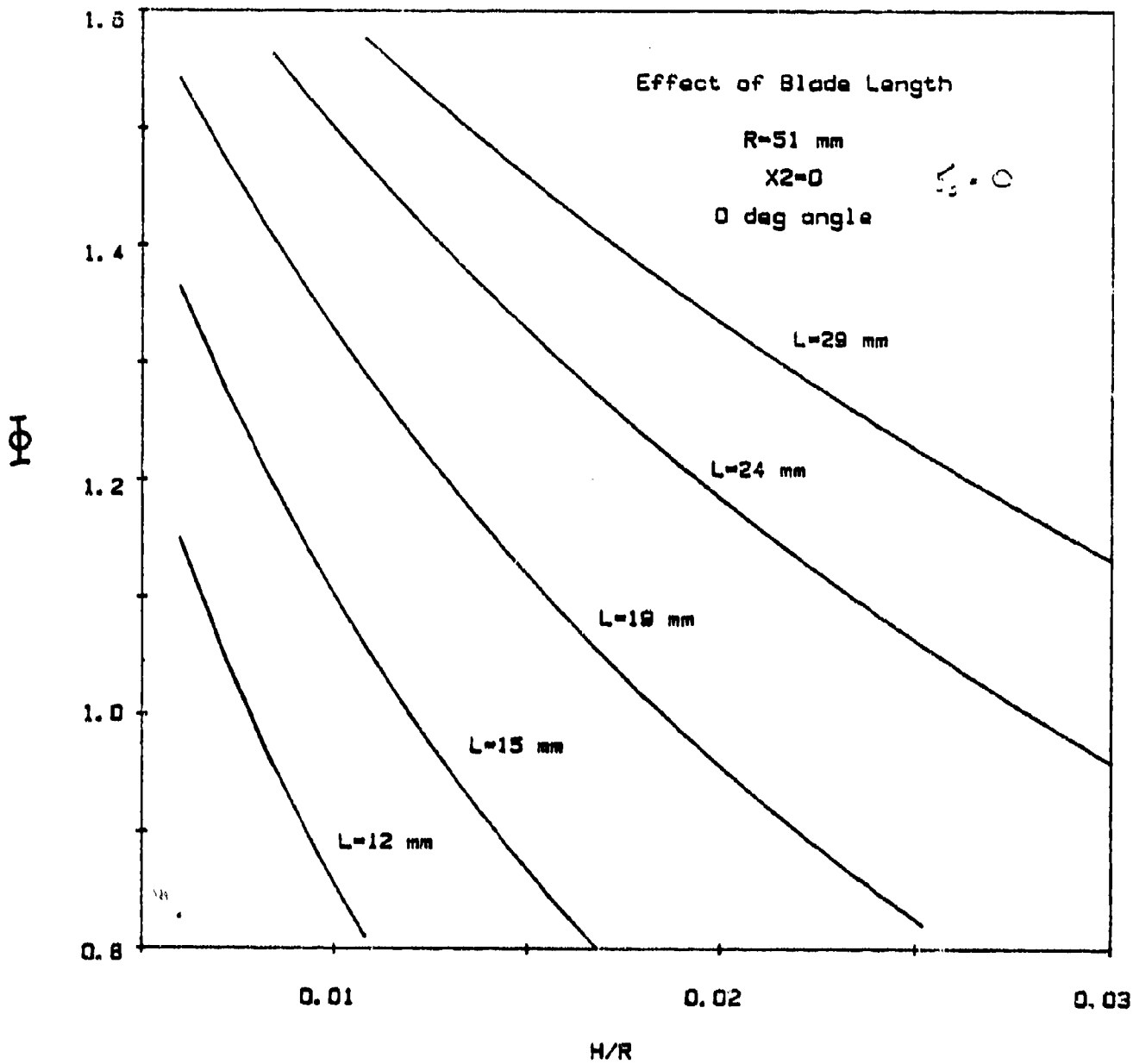

FIGURE 8: Effect of blade length on Blade Loading
Solid lines are Lubrication Theory
for a Newtonian liquid.

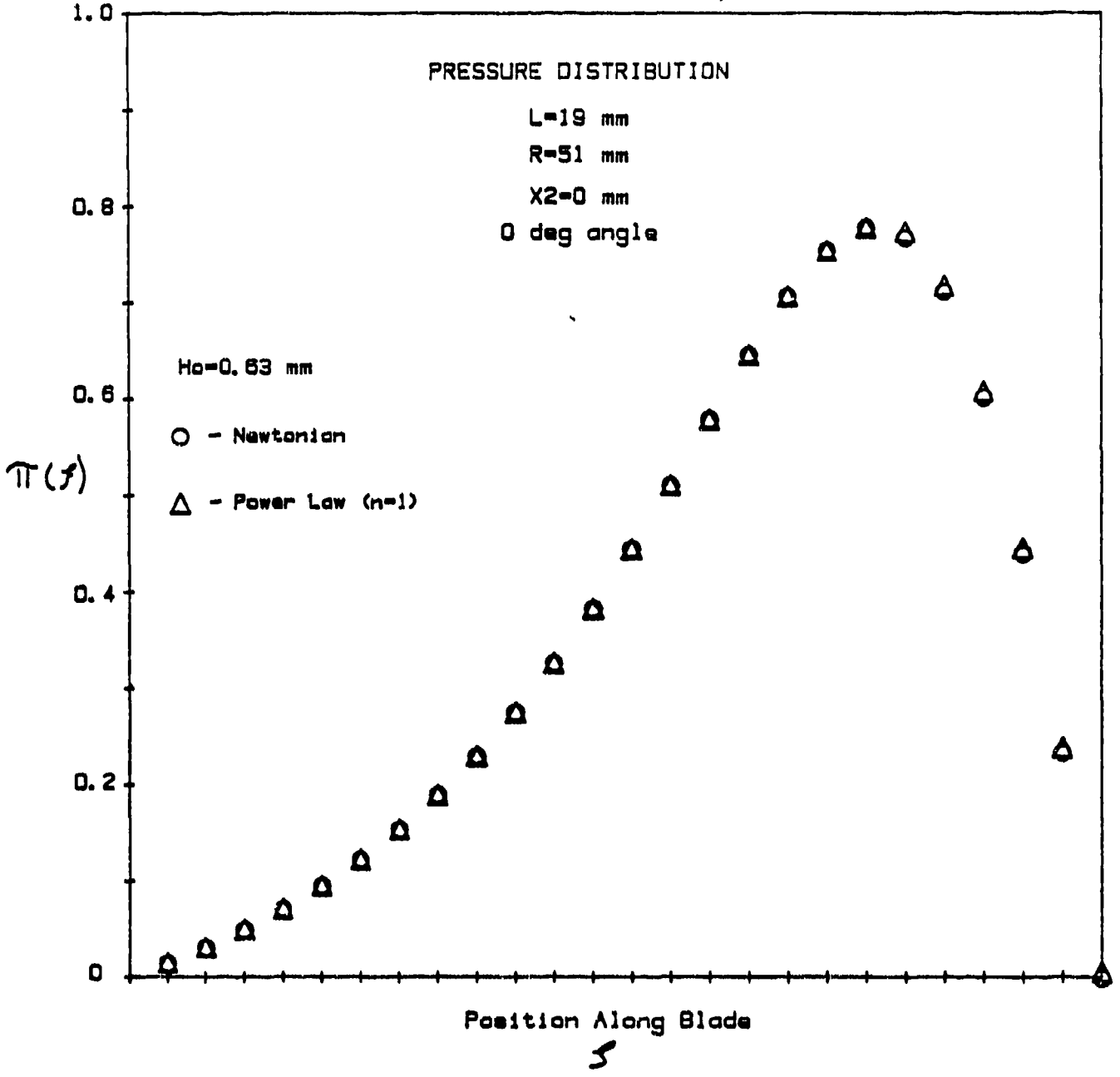

FIGURE 9a: Comparison of the Pressure Distribution under the blade obtained with the numerical Power-law Lubrication Theory algorithm (n=1) to the analytical Newtonian Lubrication Theory solution.

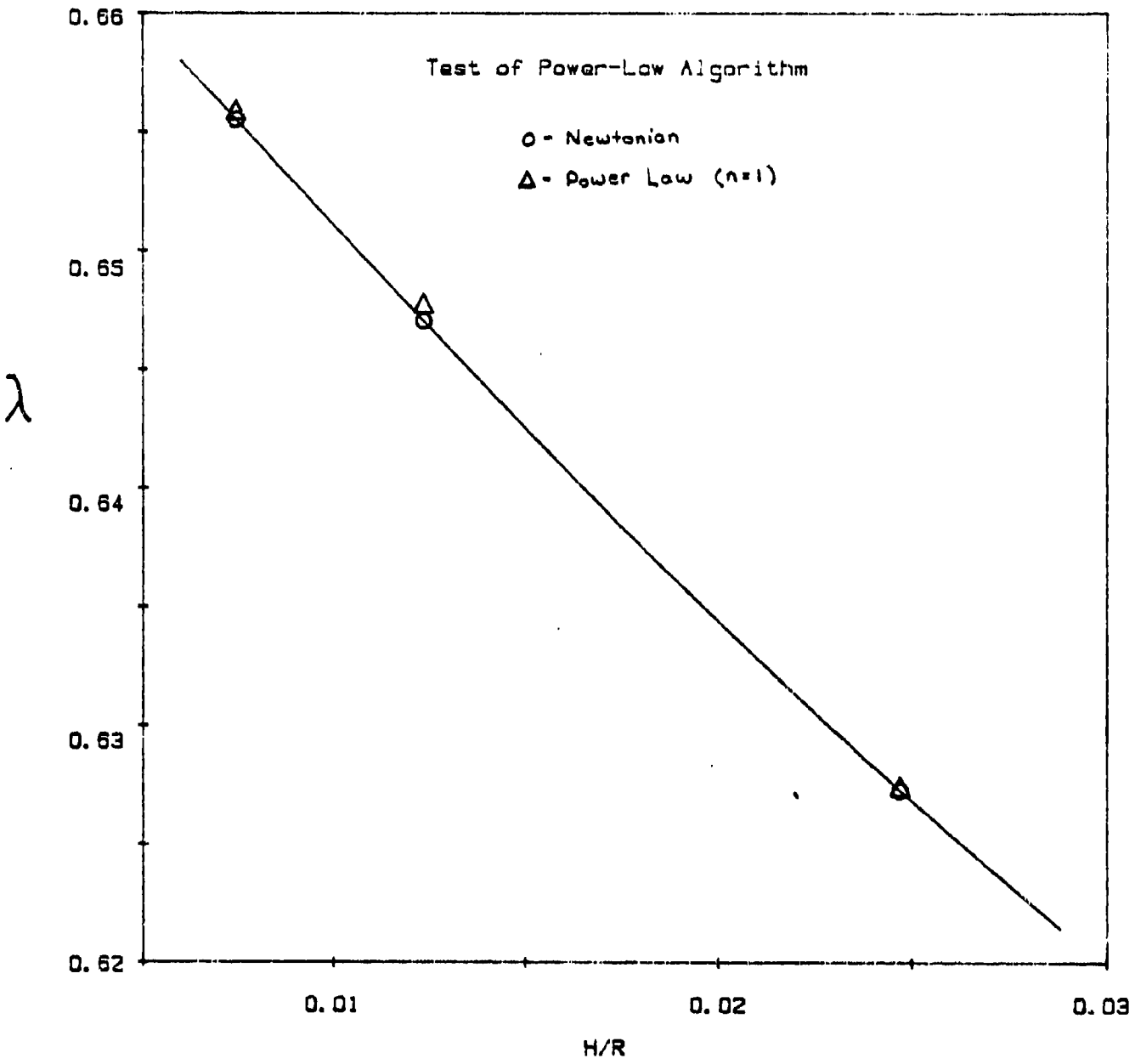

FIGURE 9b: Comparison of the Residual Fluid Thickness obtained with the numerical Power-law Lubrication Theory algorithm (n=1) to the analytical Newtonian Lubrication Theory solution.

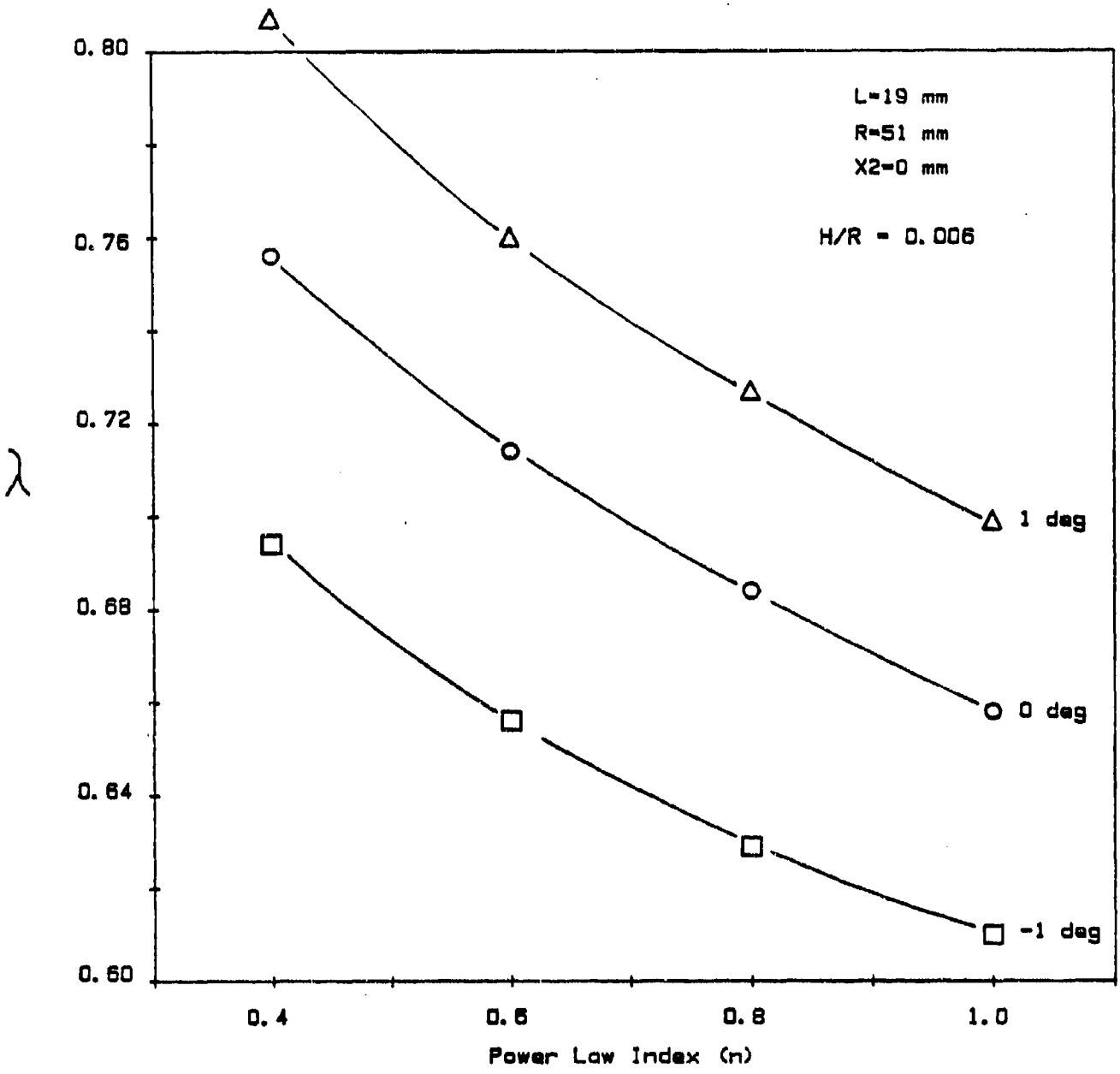

FIGURE 10: Effect of power-law index on Residual Fluid Thickness with blade angle as a parameter. (Key in Table 1)

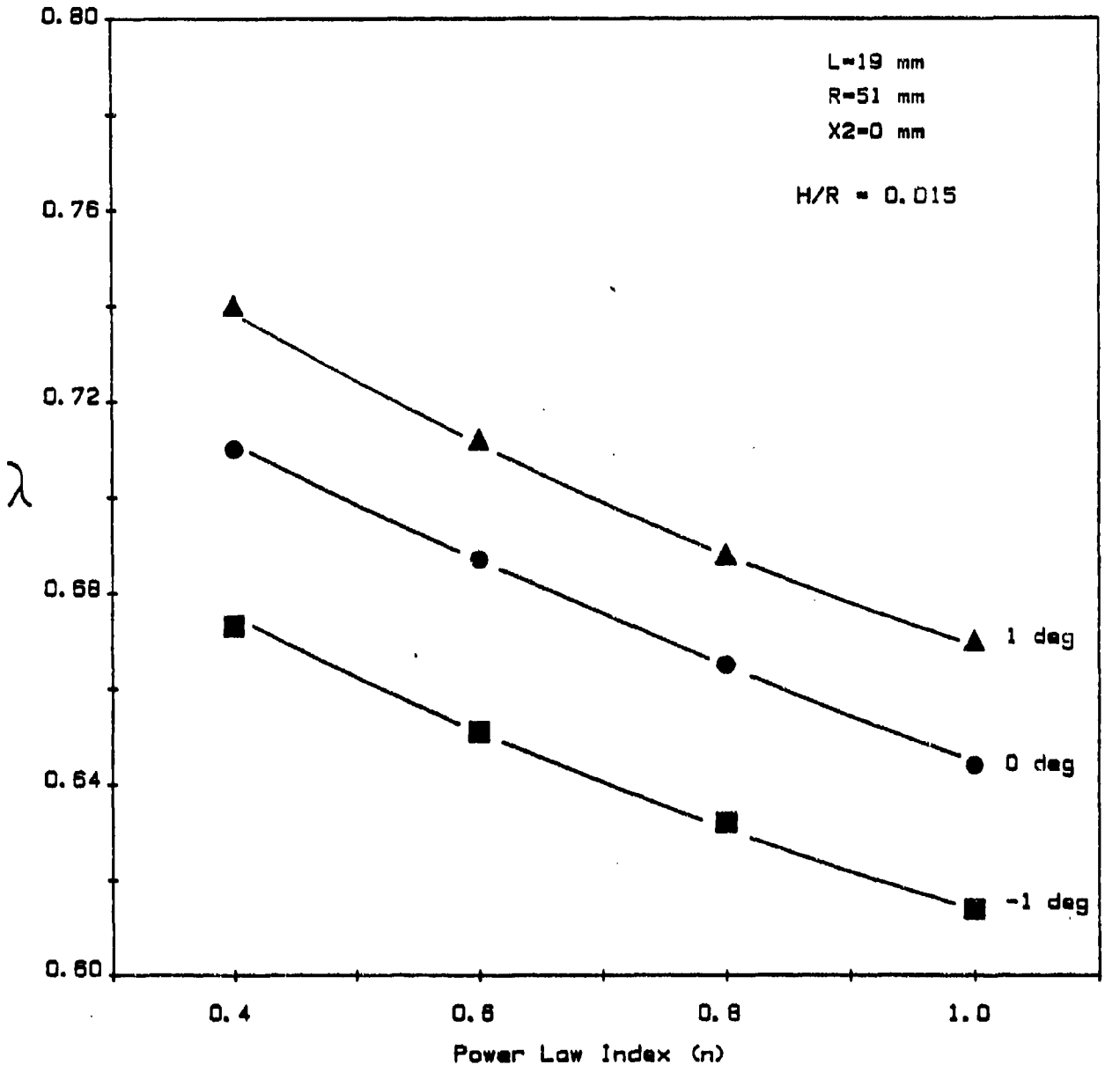

FIGURE 11: Effect of power-law index on Residual Fluid Thickness with blade angle as a parameter. (Key in Table 1)

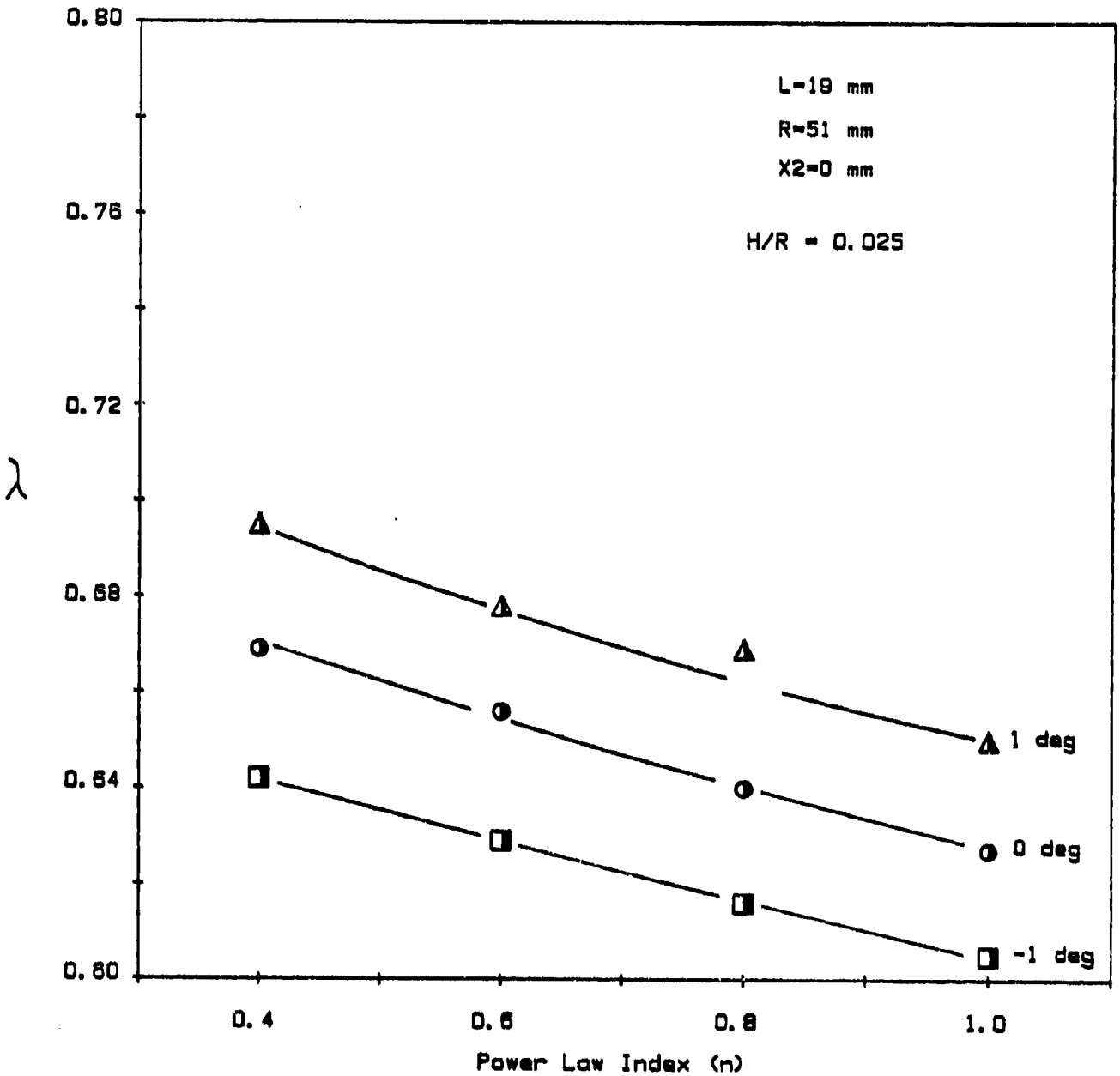

FIGURE 12: Effect of Power-law index on Residual Fluid Thickness with blade angle as a parameter. (Key in Table 1)

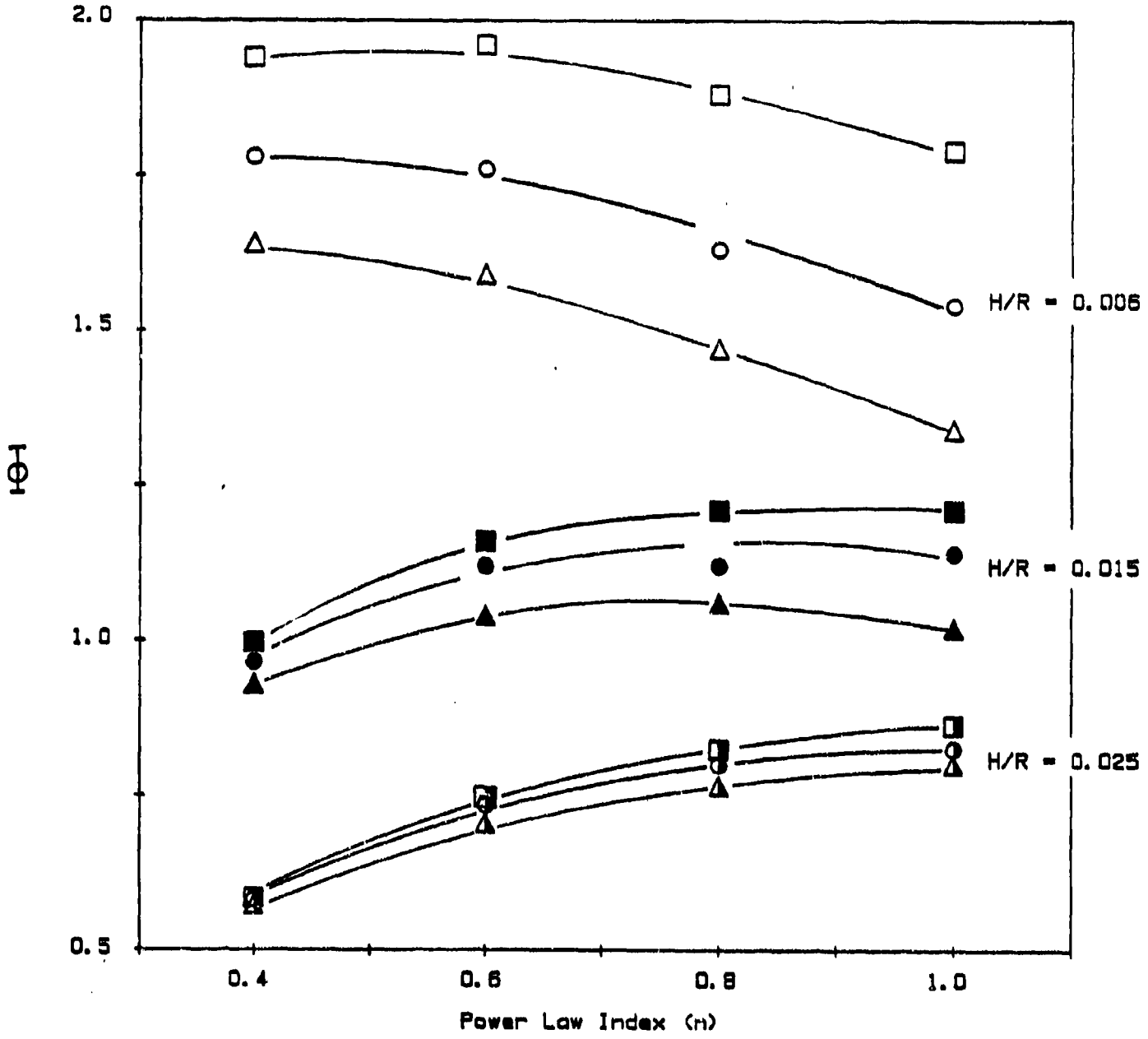

FIGURE 13: Effect of Power-law index on Blade Loading with blade angle and blade height as parameters. (Key in Table 1)

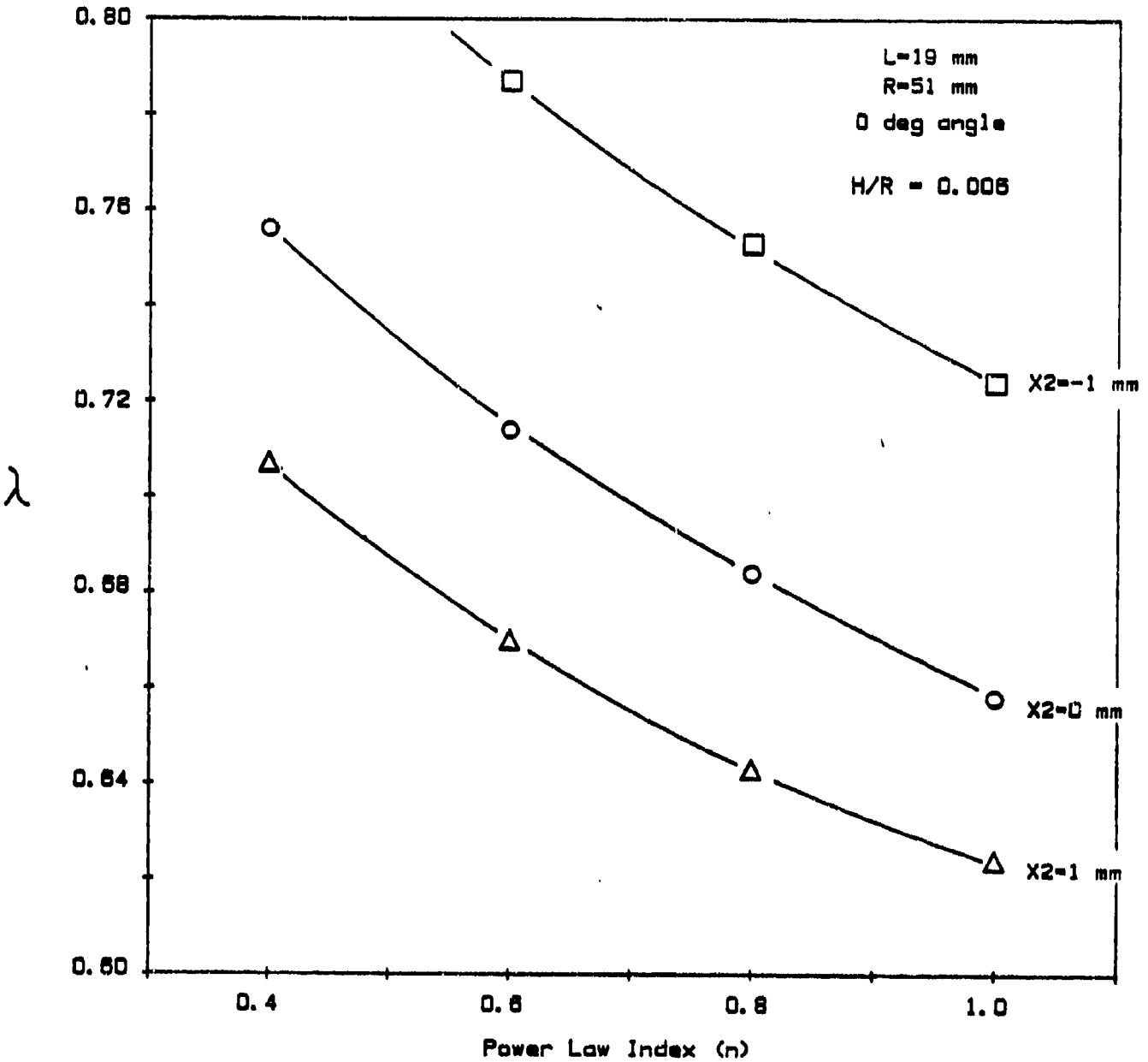

FIGURE 14: Effect of Power-law index on Residual Fluid Thickness with blade displacement as a parameter. (Key in Table 1)

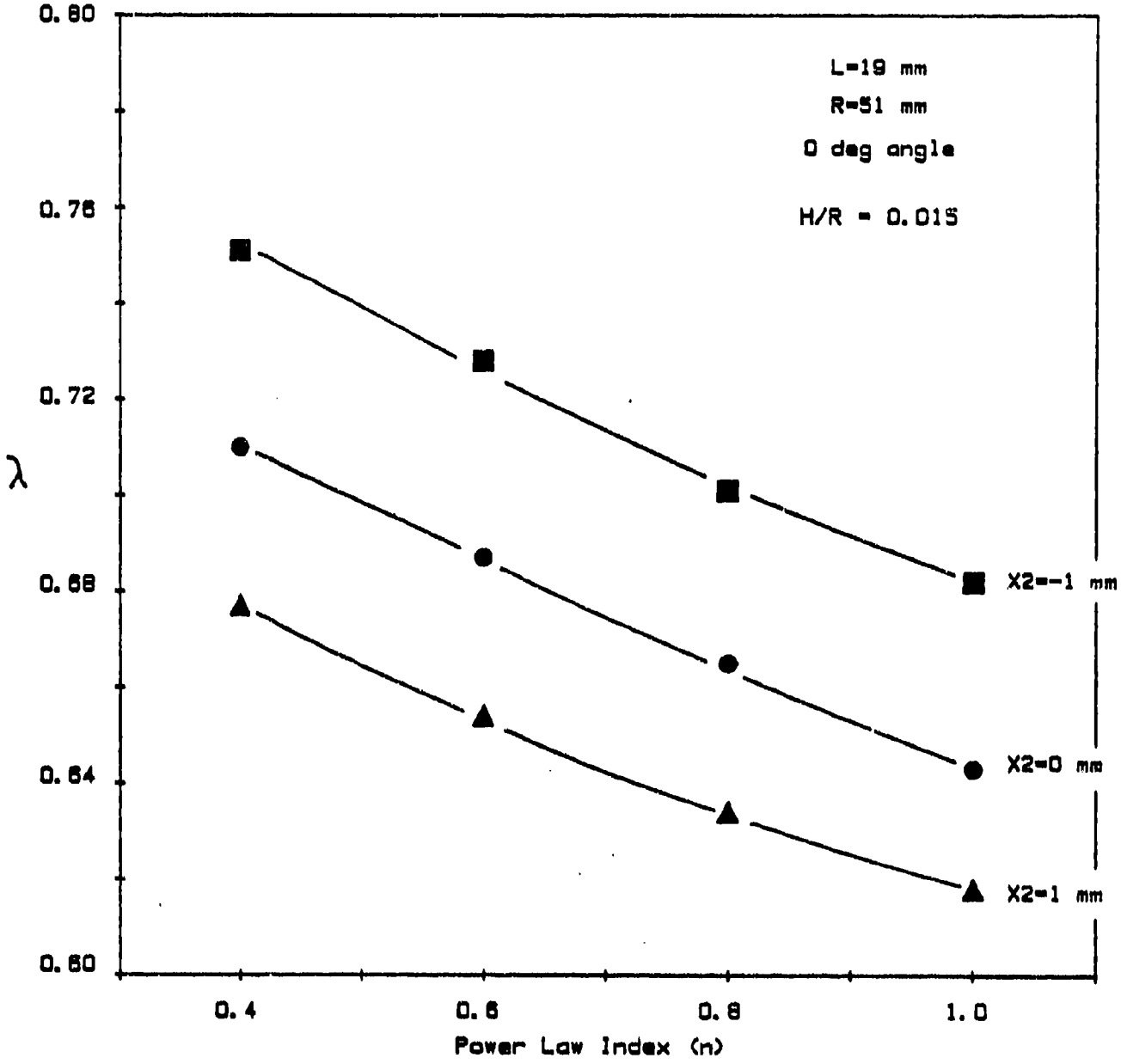

FIGURE 15: Effect of Power-law index on Residual Fluid Thickness with blade displacement as a parameter. (Key in Table 1)

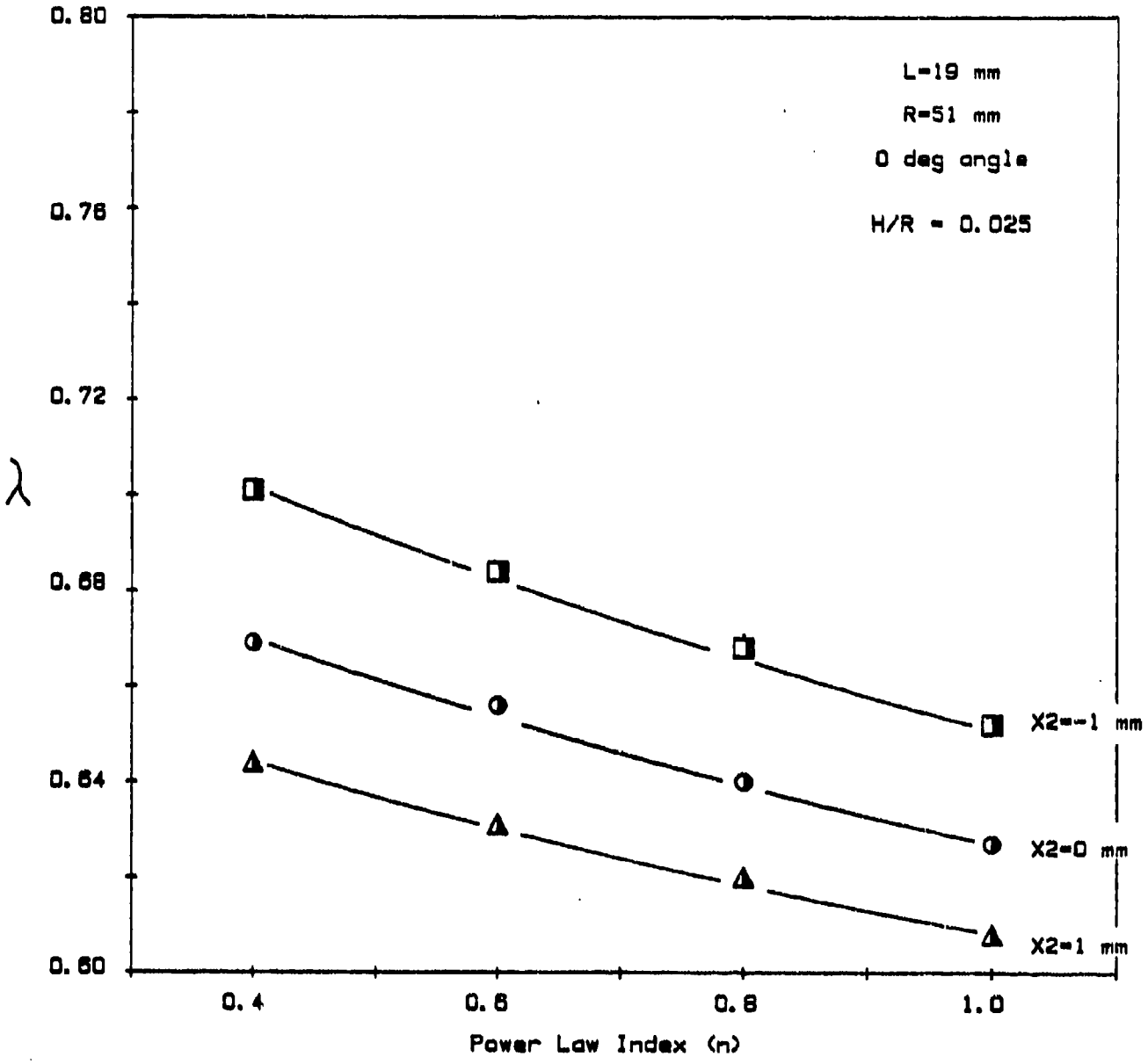

FIGURE 16: Effect of Power-law index on Residual Fluid Thickness with blade displacement as a parameter. (Key in Table 1)

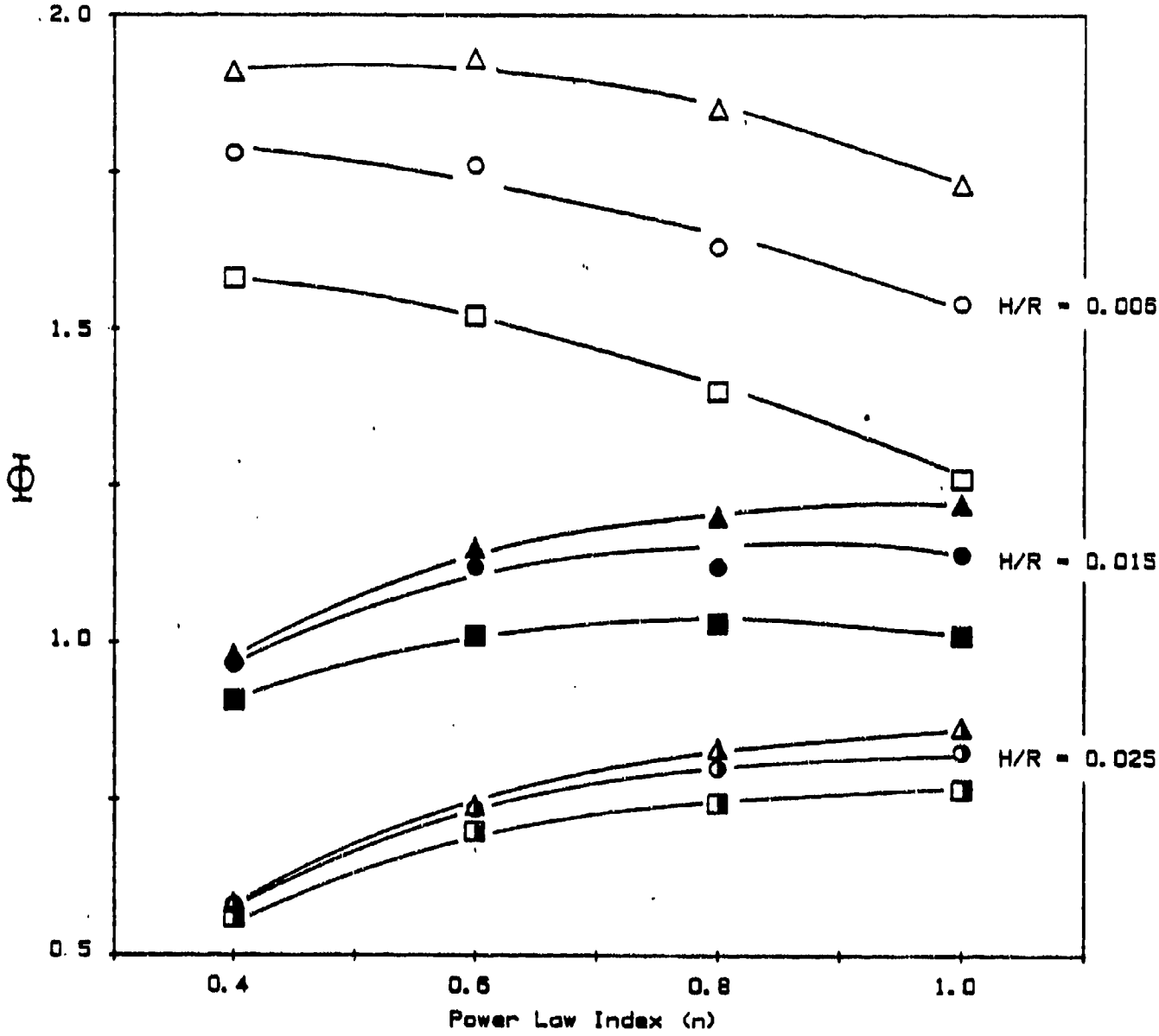

FIGURE 17: Effect of Power-law index on Blade Loading with blade displacement and blade height as parameters. (Key in Table 1)

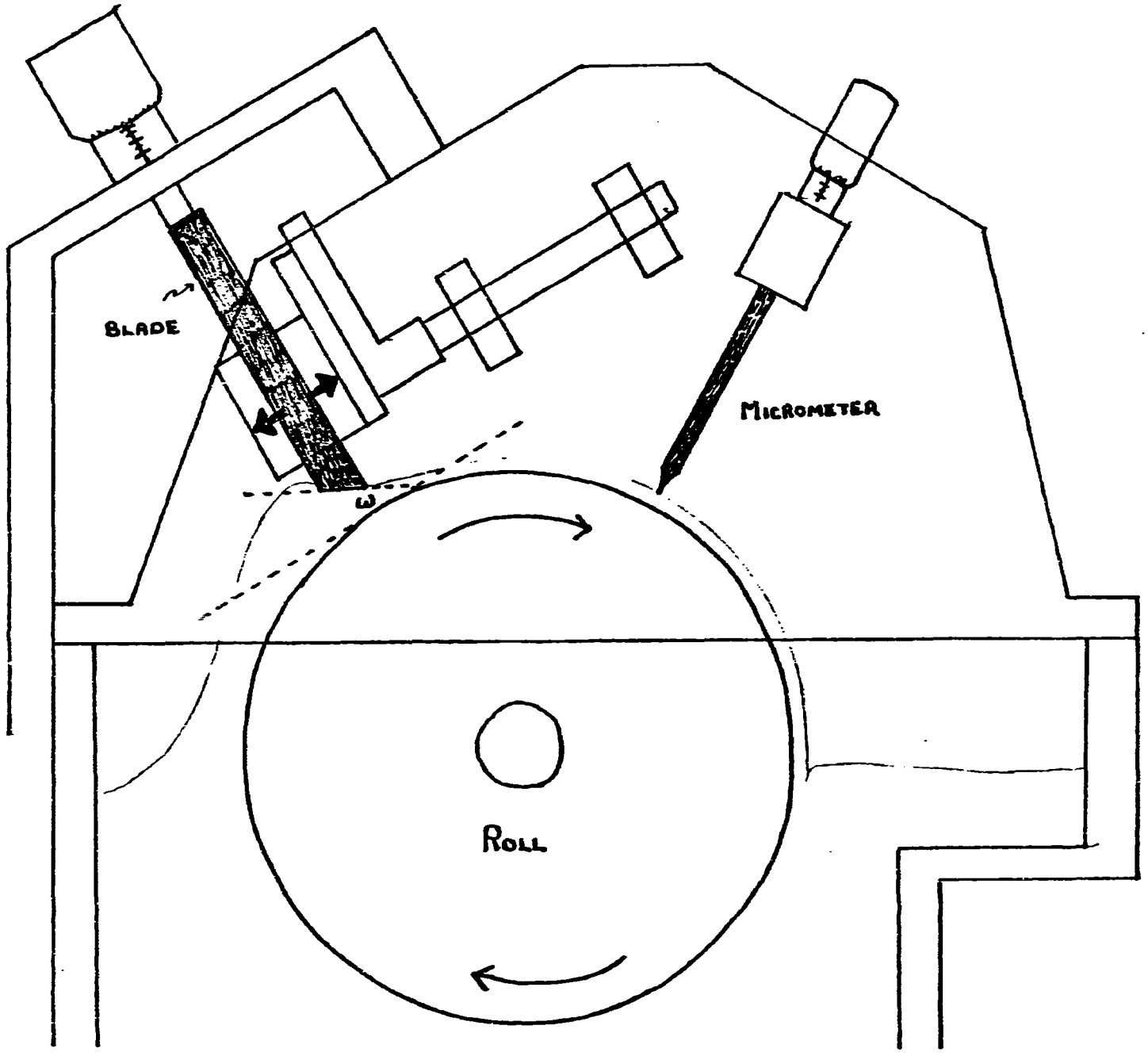

FIGURE 18: Experimental Wiping Apparatus

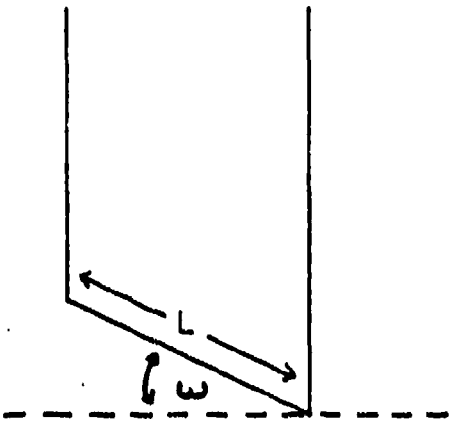

FIGURE 19: Blade Geometry - Length (L) and Angle (ω) are adjustable.

[Note: L is the land length]

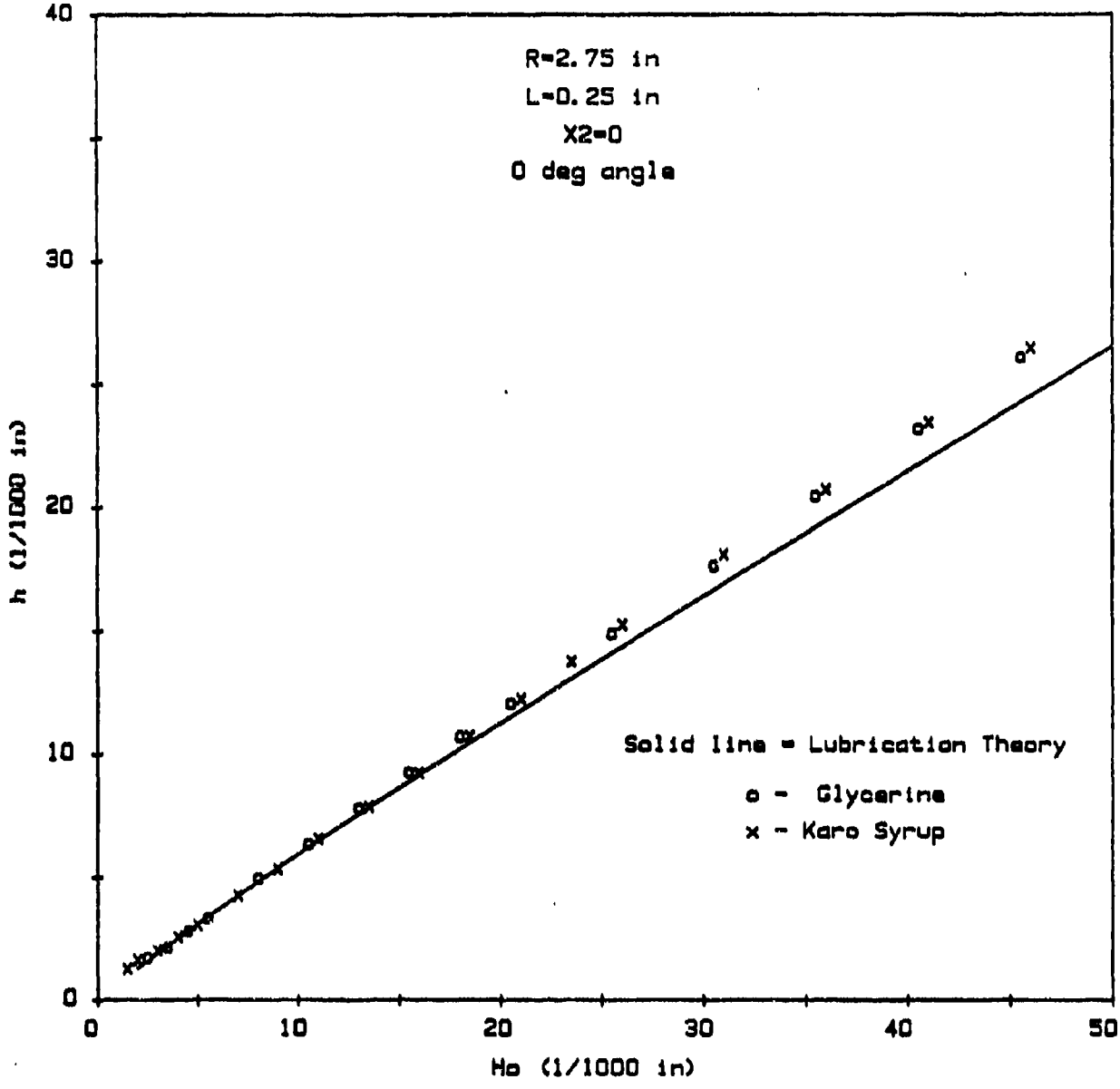

FIGURE 20: Residual Fluid Thickness vs. Blade Height for Glycerine (o) and Karo Syrup (x) compared to Lubrication Theory (line)

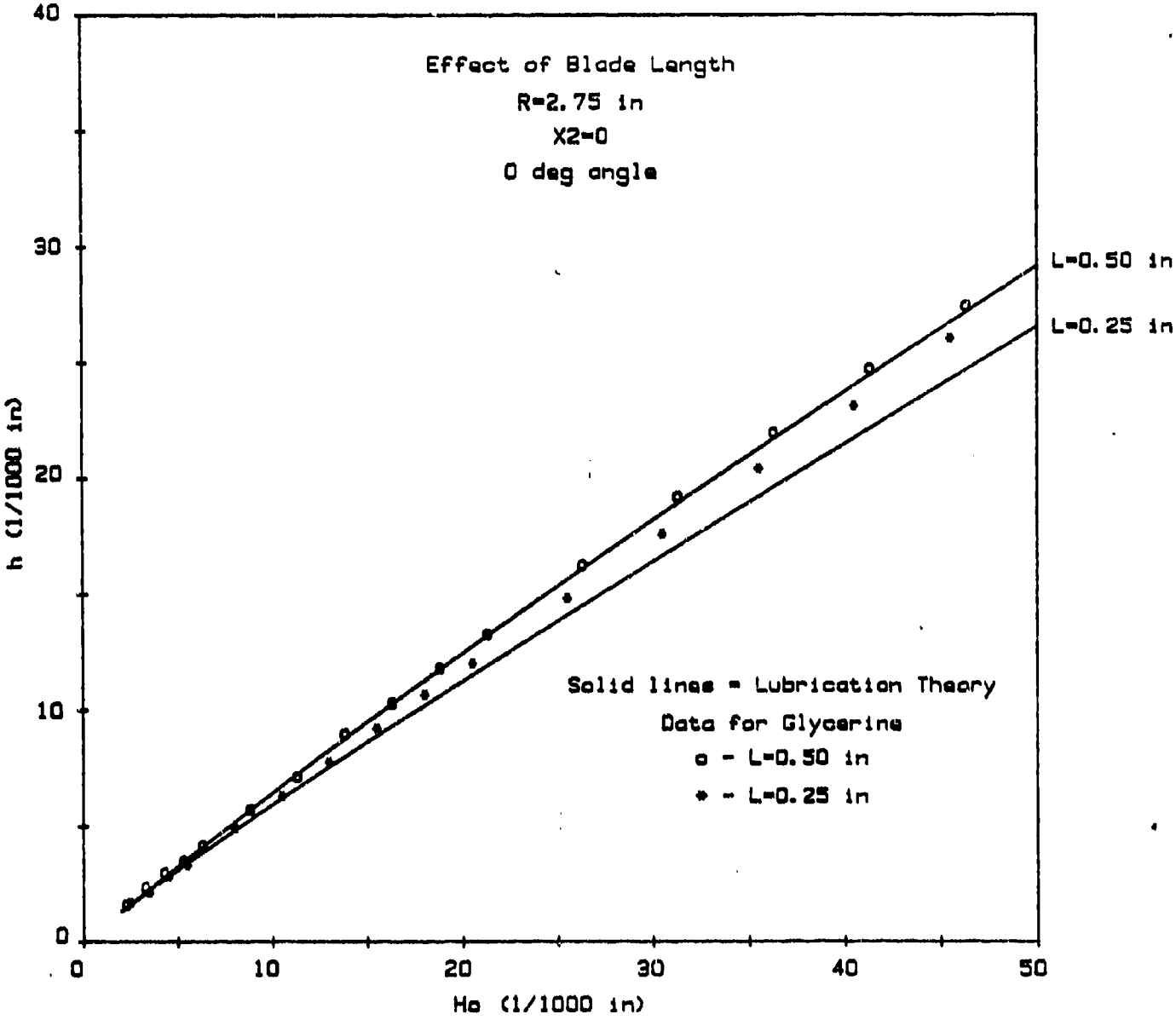

FIGURE 21: Newtonian data and Lubrication Theory showing the effect of blade length.

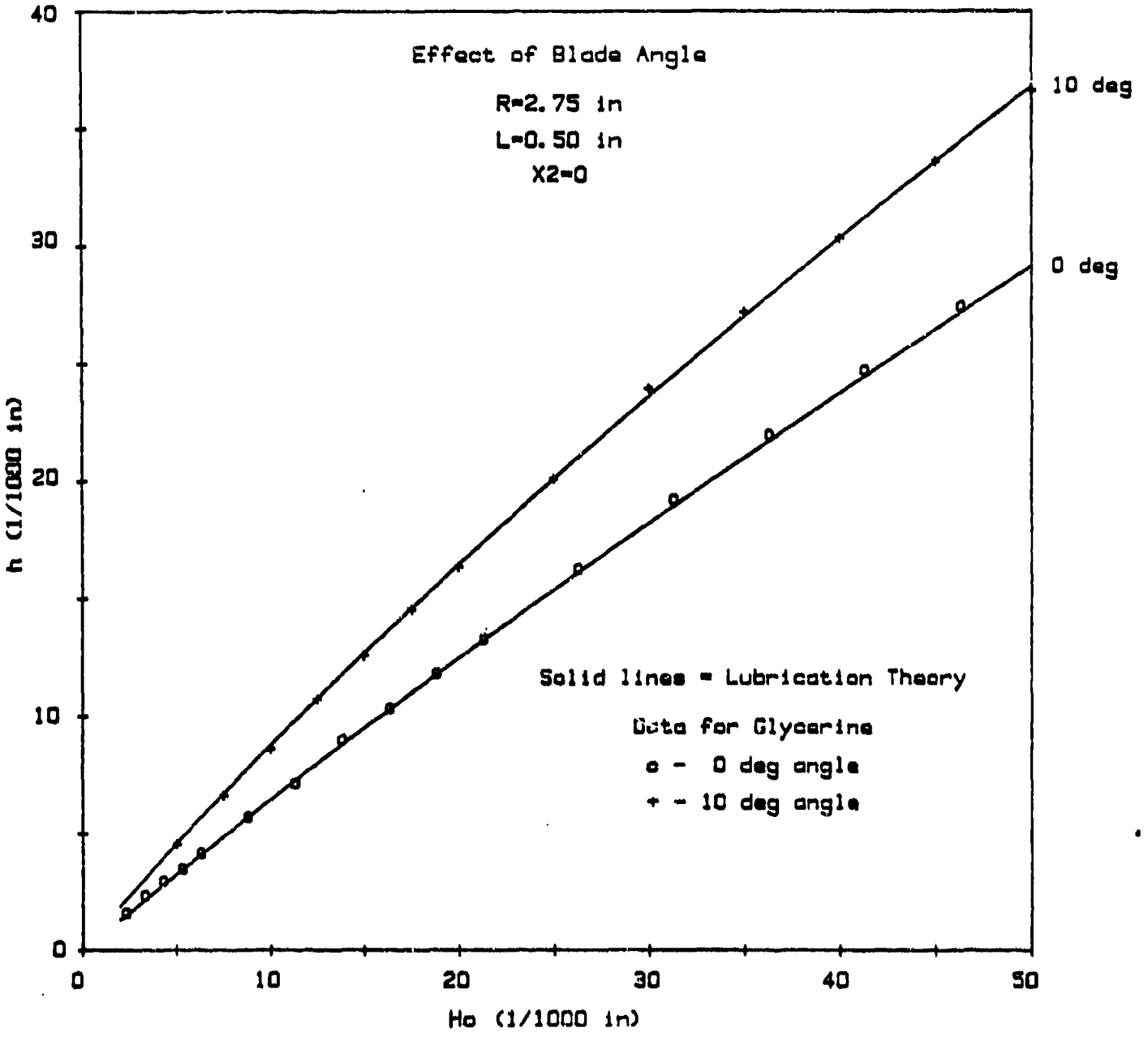

FIGURE 22: Newtonian data and Lubrication Theory showing the effect of blade angle using a 1/2 in. blade.

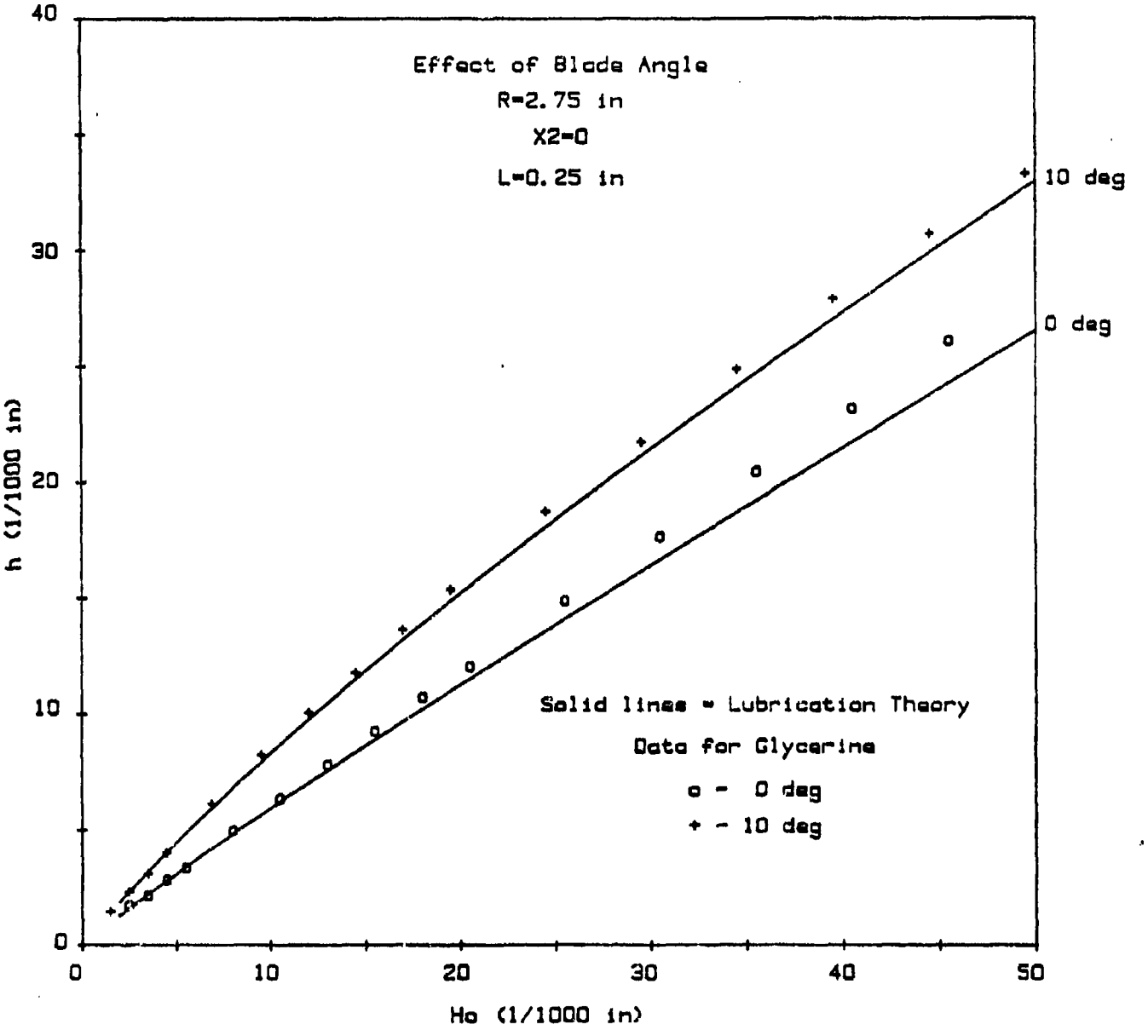

FIGURE 23: Newtonian data and Lubrication Theory showing the effect of blade angle using a 1/4 in. blade.

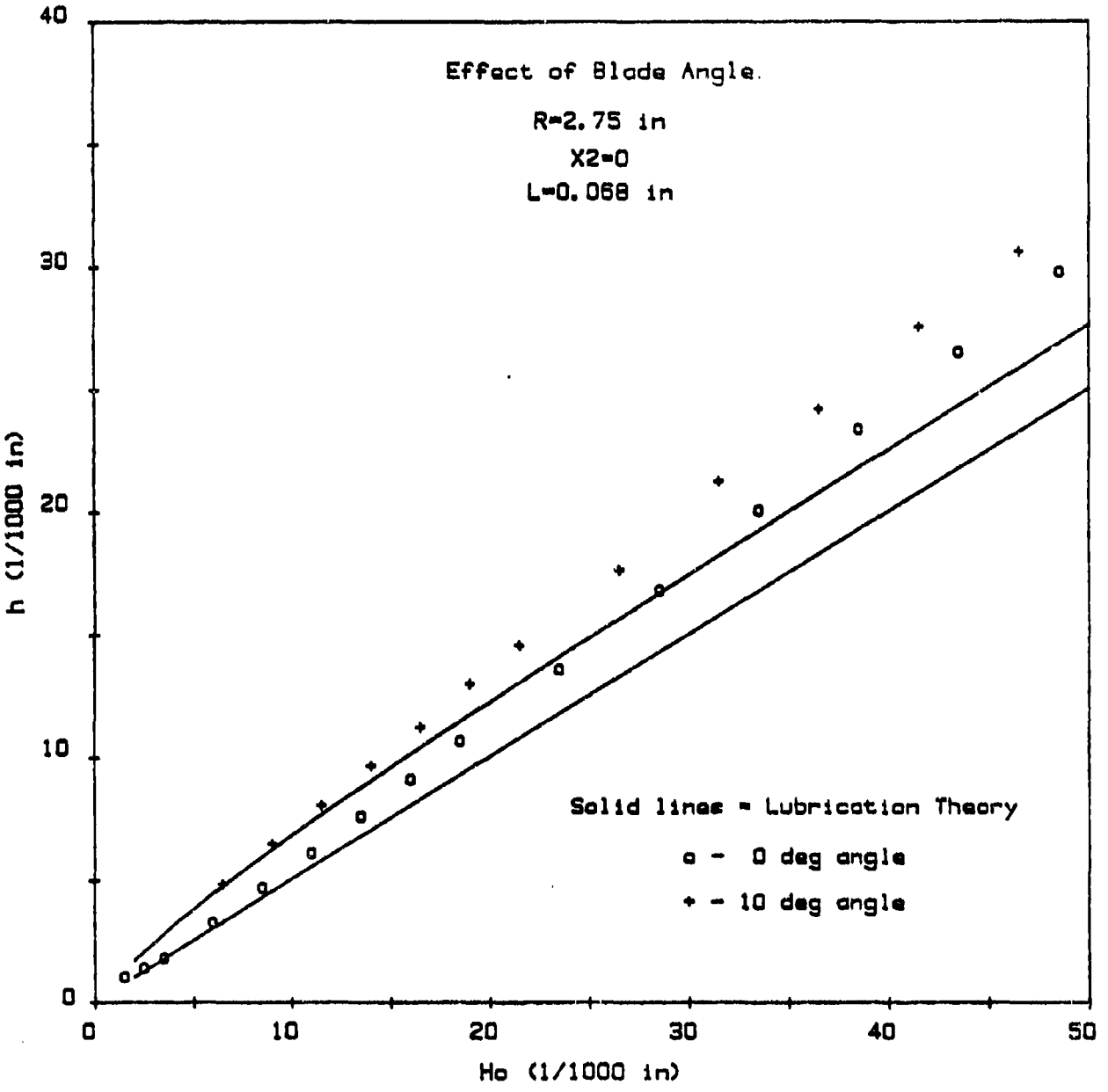

FIGURE 24: Newtonian data and Lubrication Theory showing the effect of blade angle using a 0.068 in. blade.

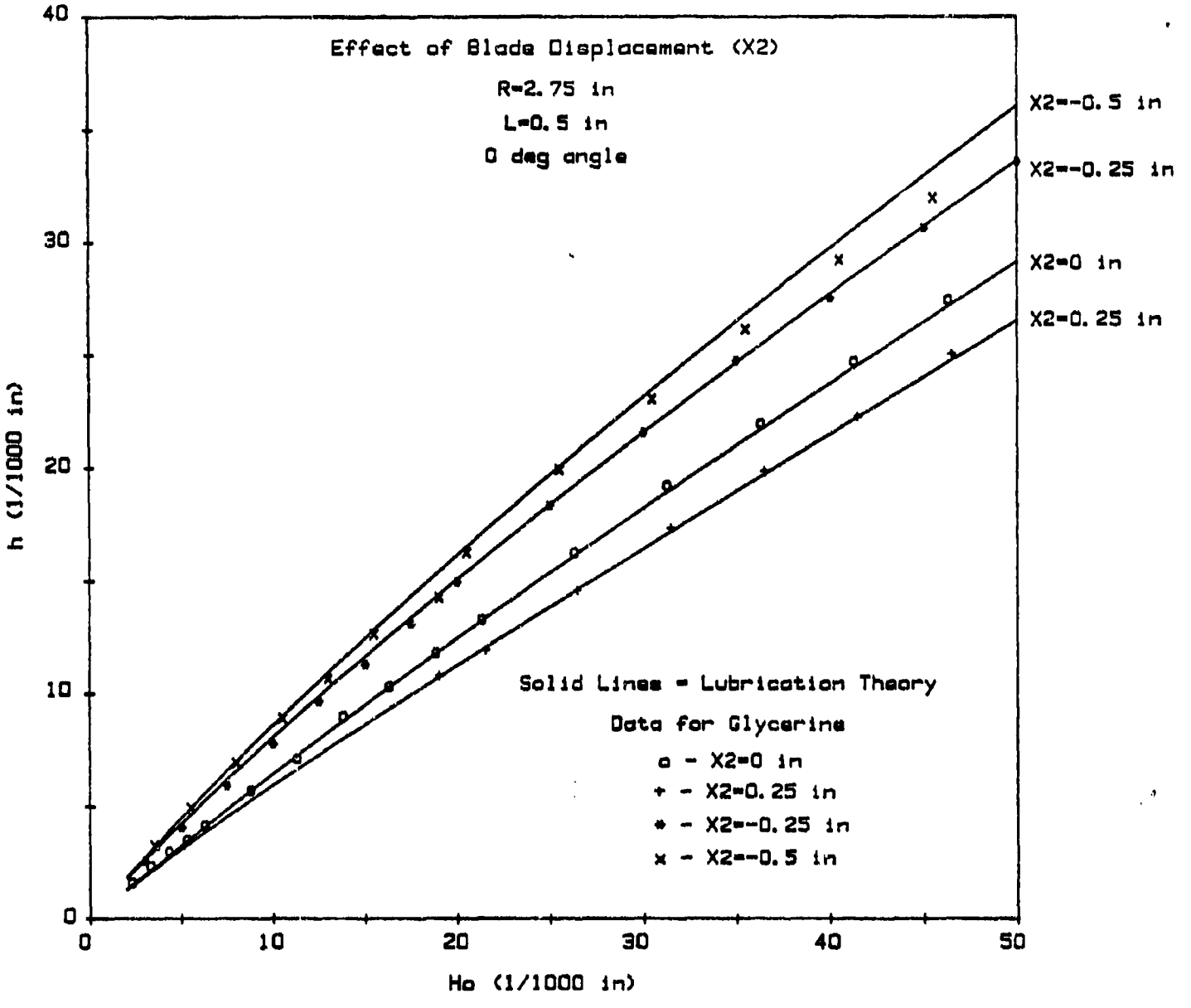

FIGURE 25: Newtonian data and Lubrication Theory showing the effect of blade displacement using a 1/2 in. blade at 0 degrees.

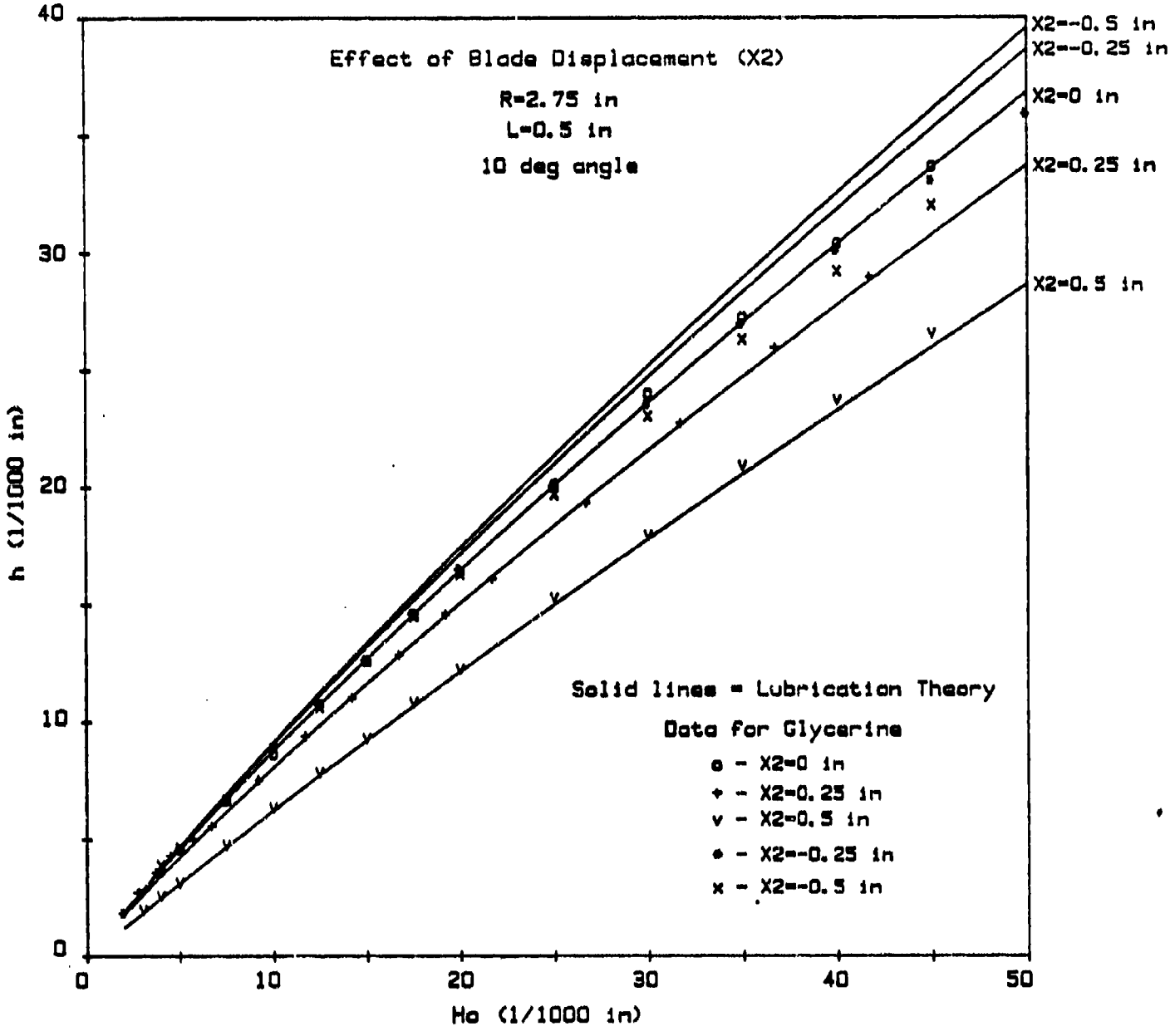

FIGURE 26: Newtonian data and Lubrication Theory showing the effect of blade displacement using a 1/2 in. blade at 10 degrees.

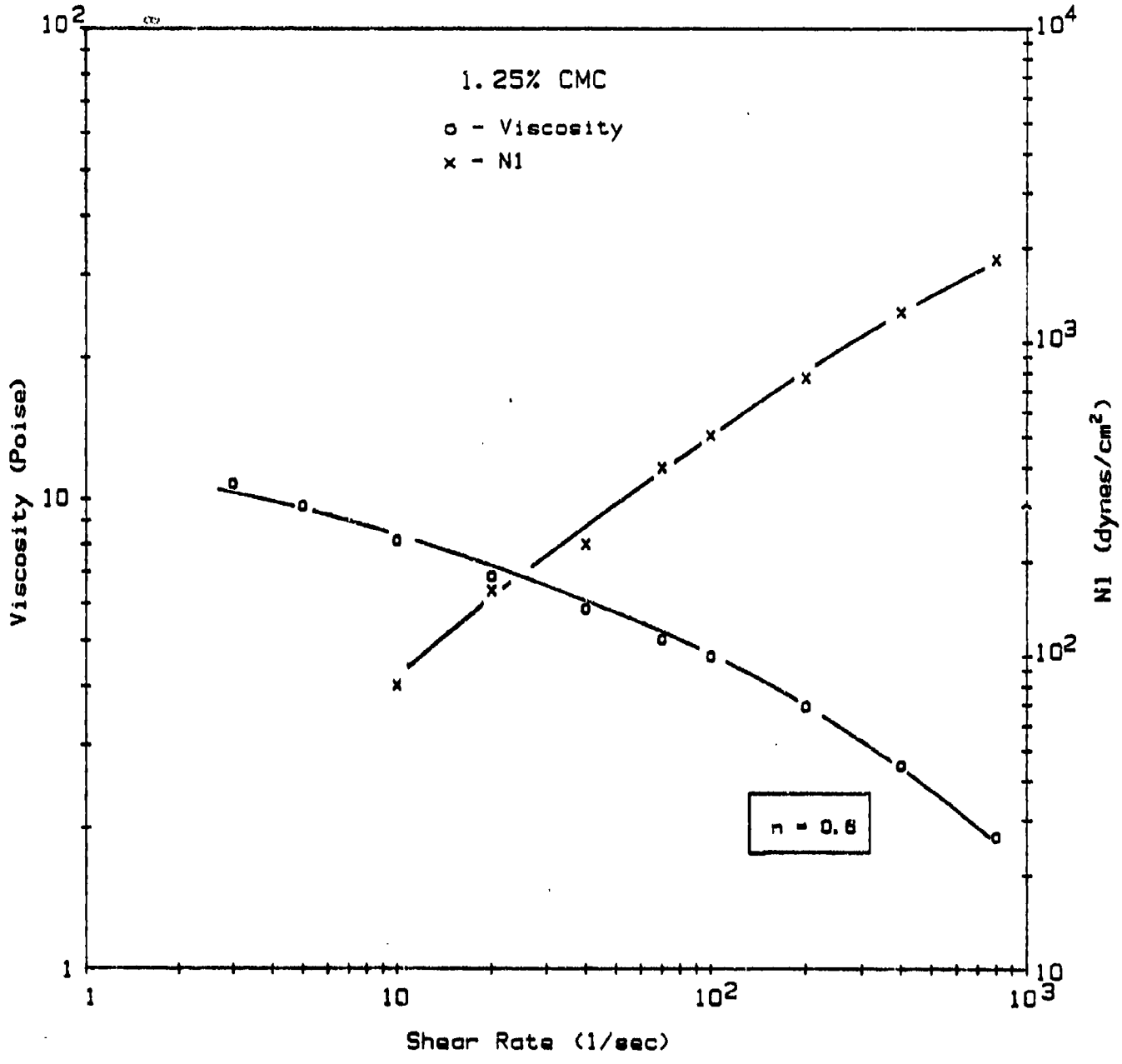

FIGURE 27: Viscosity and Normal Stress vs. Shear Rate for 1.25% CMC solution.

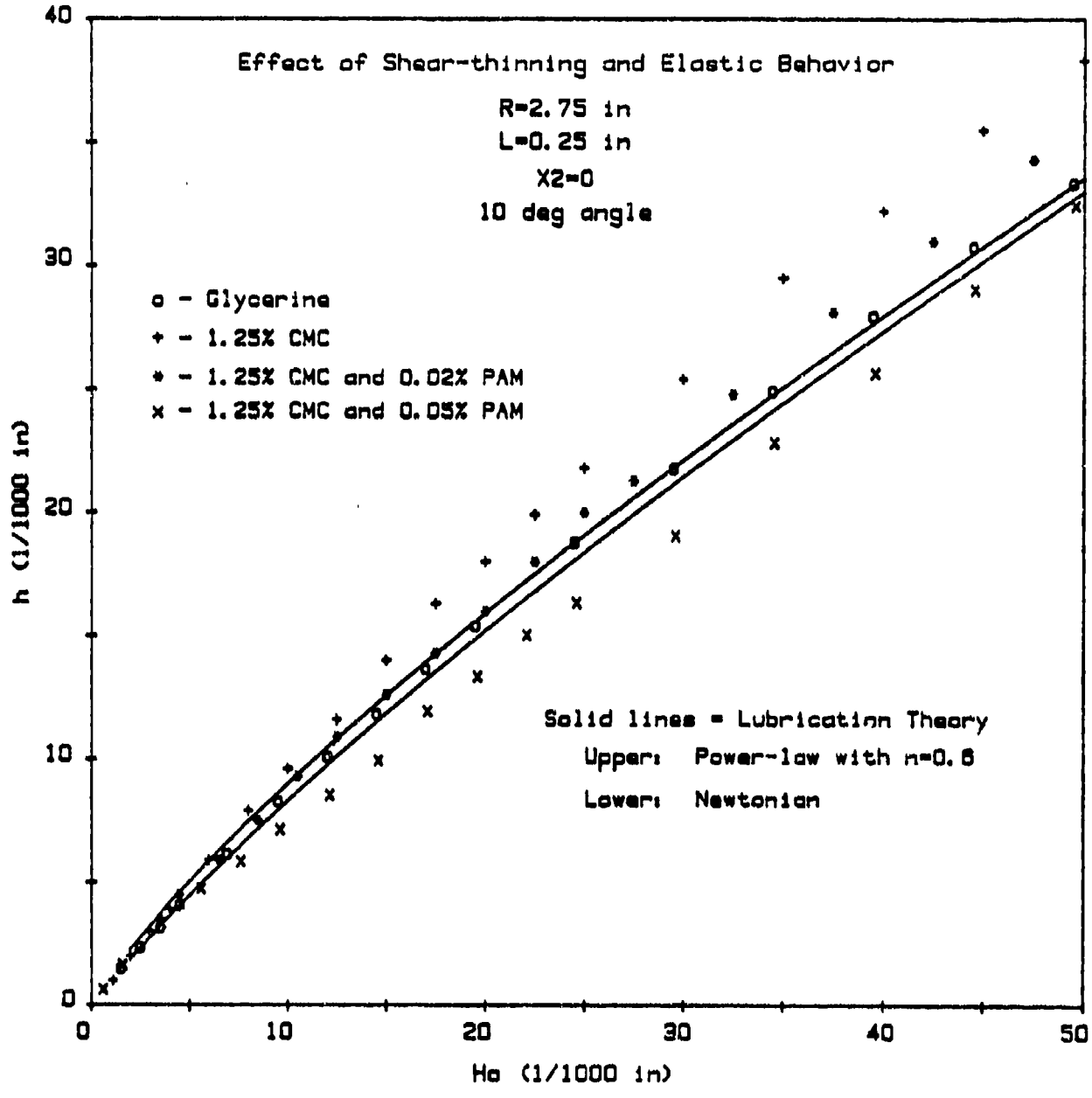

FIGURE 28: Data for Newtonian and Viscoelastic liquids compared to Newtonian and Power-law Lubrication Theory.

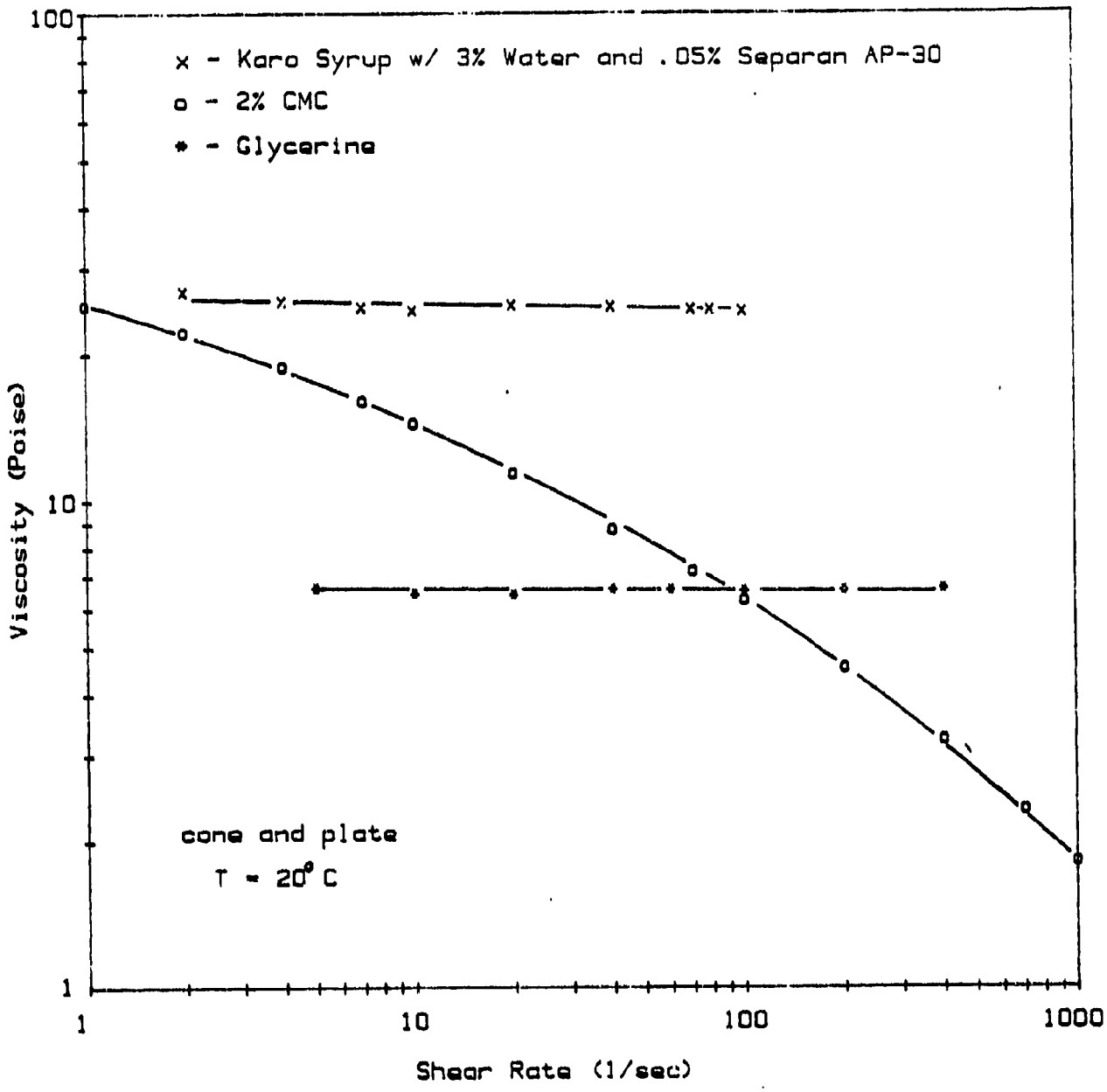

FIGURE 29: Viscosity vs. Shear Rate for Boger Fluid (x), 2% CMC (o), and Glycerine (*).

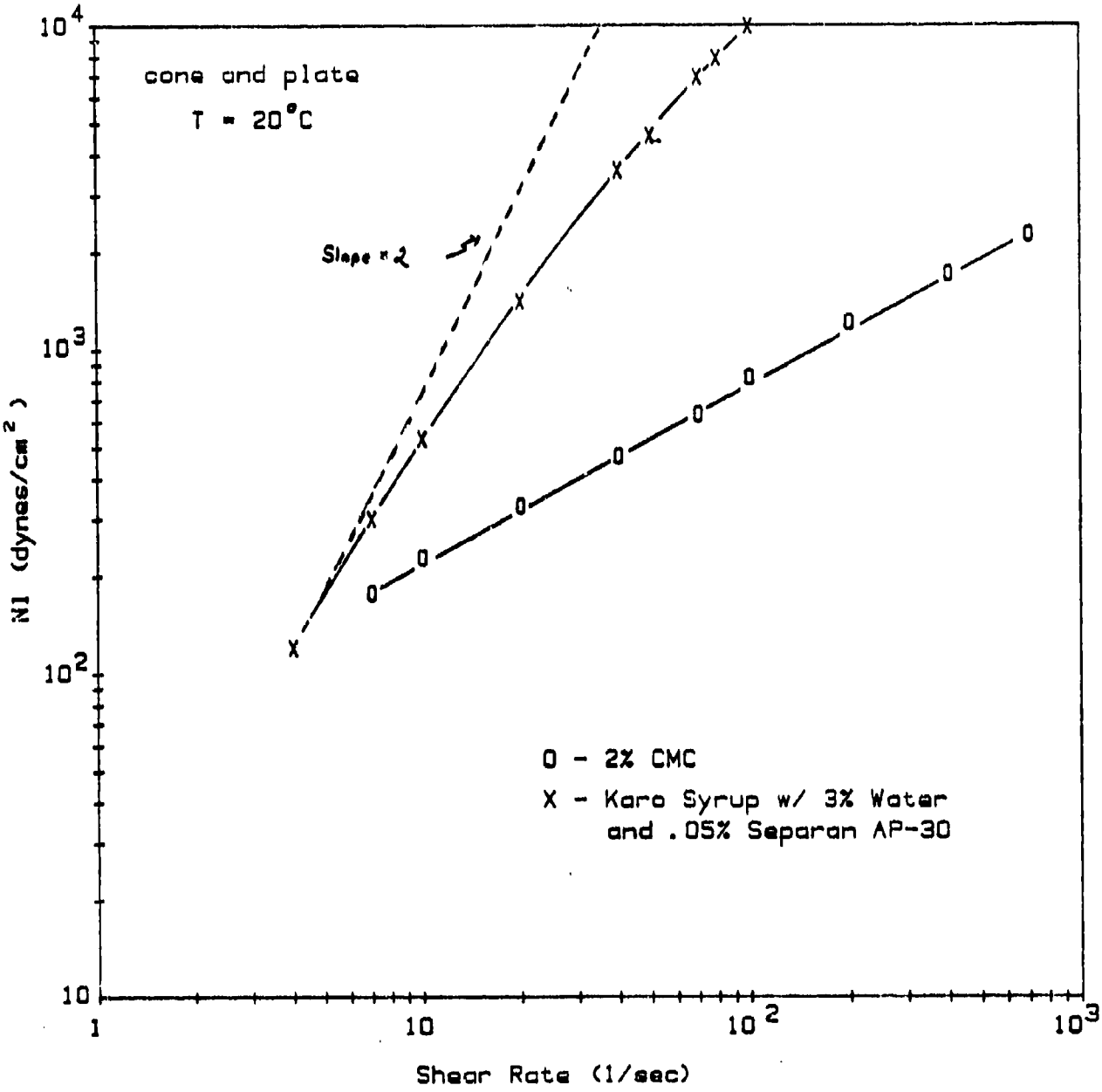

FIGURE 31: Normal Force vs. Shear Rate for Boger Fluid (x) and 2% CMC (o).

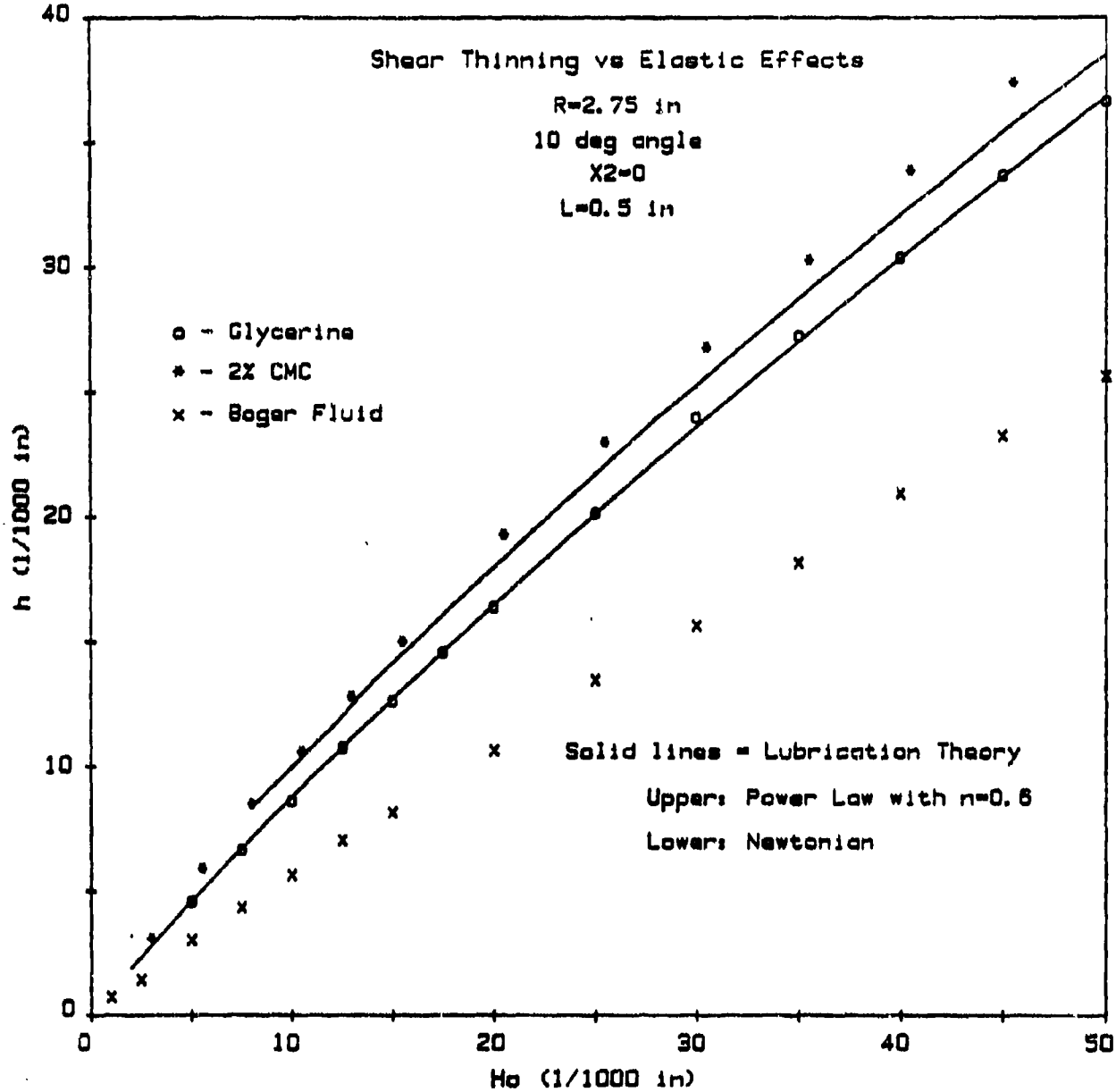

FIGURE 31: Data for Newtonian and Viscoelastic liquids compared to Newtonian and Power-law Lubrication Theory.

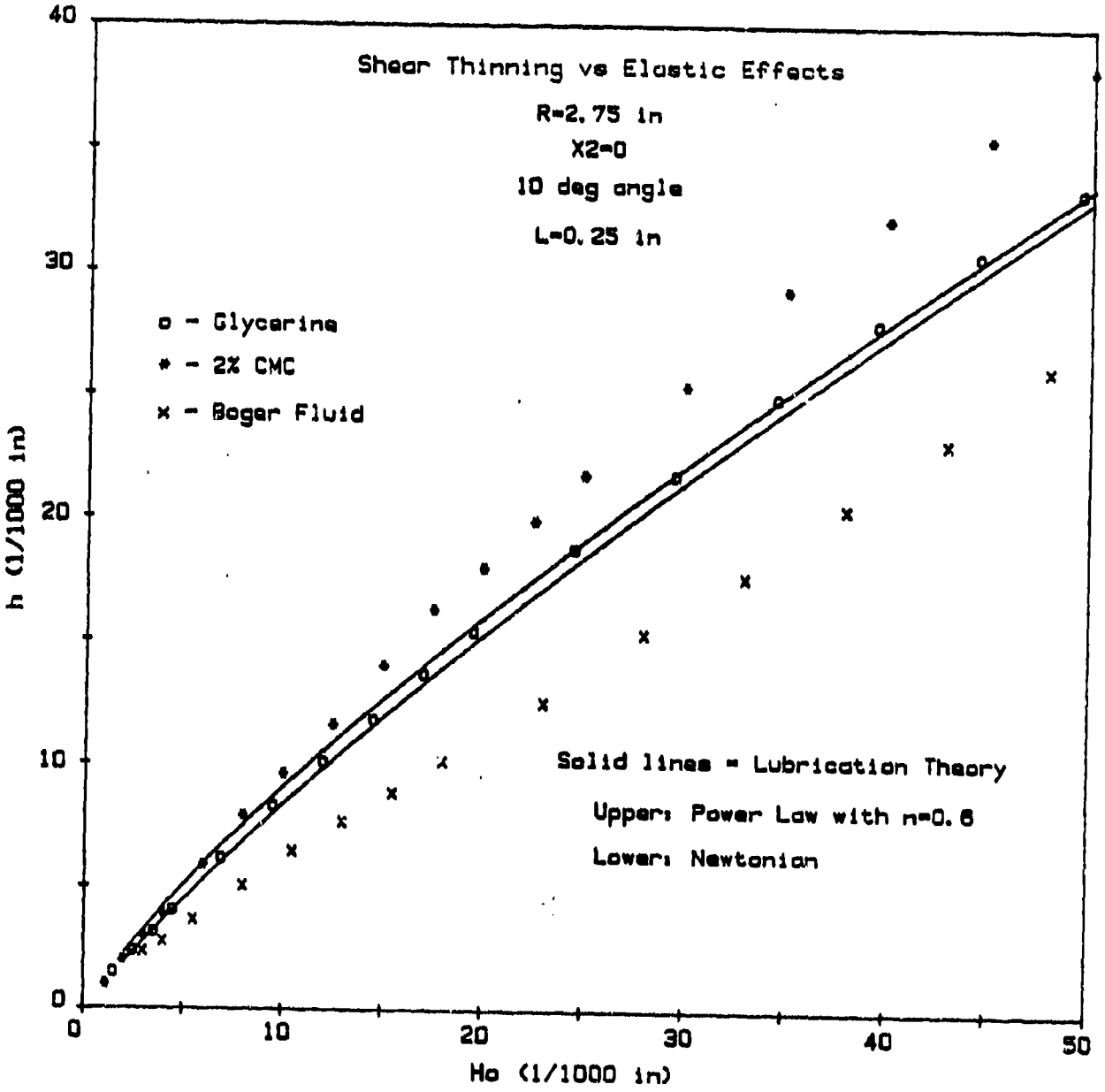

FIGURE 32: Data for Newtonian and Viscoelastic liquids compared to Newtonian and Power-law Lubrication Theory.

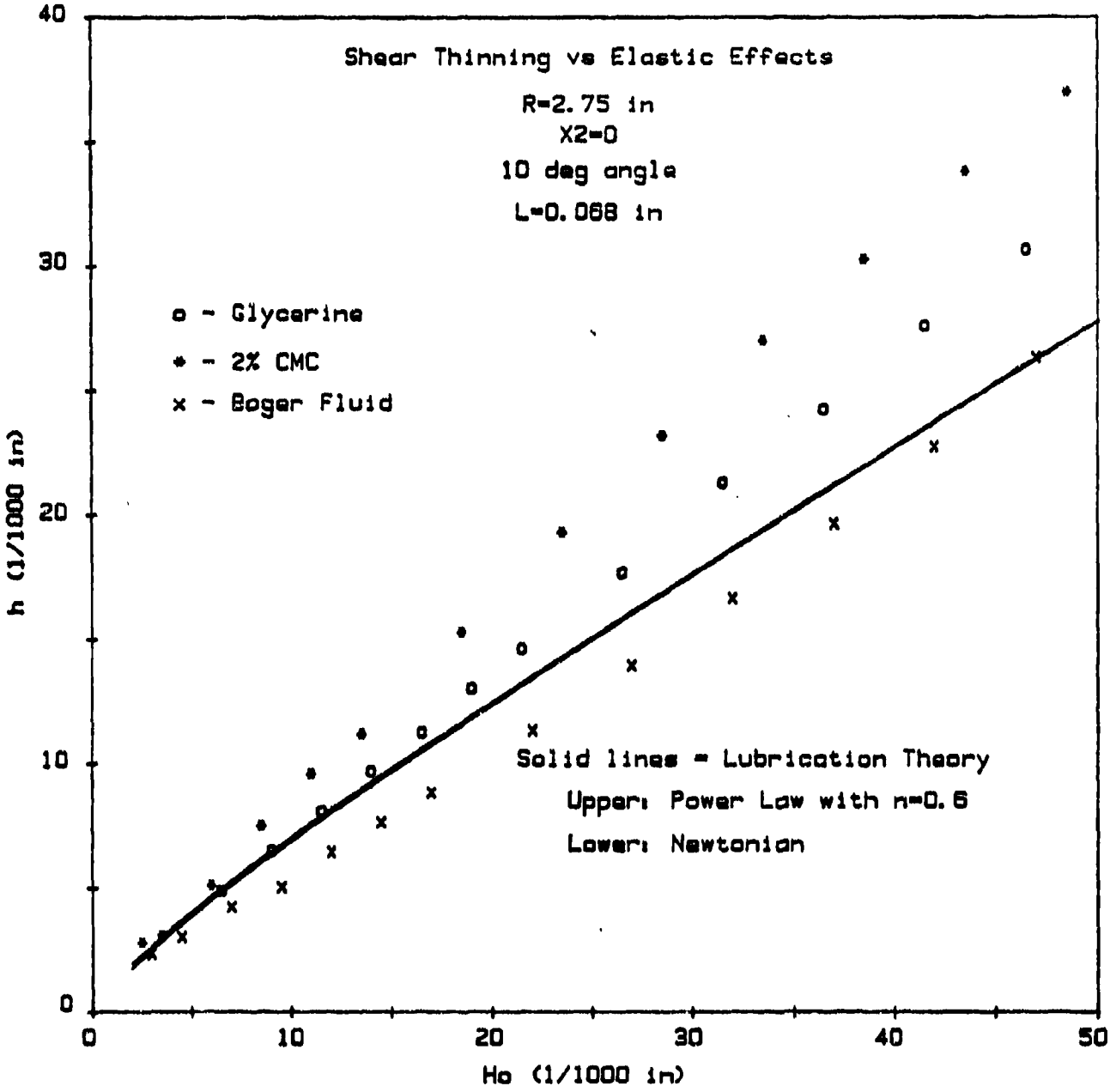

FIGURE 33: Data for Newtonian and Viscoelastic liquids compared to Newtonian and Power-law Lubrication Theory.

REFERENCES

(1) Bauman, T., T. Sullivan, and S. Middleman, "Ribbing Instability in Coating Flows: Effect of Polymer Additives", Chem. Eng. Commun., 14 35 (1982).

(2) Bird, R.B., W.E. Stewart, and E.N. Lightfoot, Transport Phenomena, John Wiley and Sons, N.Y. (1960).

(3) Boger, D. V., "A Highly Elastic Constant-Viscosity Fluid", J. Non-Newt. Fluid Mech. 3 87 (1977).

(4) Boger, D. V., "Separation of Shear Thinning and Elastic Effects in Experimental Rheology", in Rheology I: Principles, Ed. by G. Astarita, G. Marucci, and L. Nicolais, Plenum Press, N.Y.(1980).

(5) Burley, R. and R. P. S. Jolly, "Entrainment of Air into Liquids by a High Speed Continuous Solid Surface", Chem. Eng. Sci., 39 1357 (1984).

(6) Cameron,A., Principles of Lubrication,Longmans, London (1966).

(7) Campanella, O.H. and R. L. Cerro, "Viscous Flow on the Outside of a Horizontal Rotating Cylinder: The Roll Coating Regime With a Single Fluid", Chem. Eng. Sci., 39 1443 (1984).

(8) Choplin, L., P. J. Carreau, and A. Ait Kadi, "Highly Elastic - Constant Viscosity Fluids", Poly. Eng. Sci., 23 459 (1983).

(9) Doremus, P. and J. M. Piau, "Viscoelastic Elongational Lubrication", J. Non-Newt. Fluid Mech., 9 389 (1981).

(10) Doremus, P. and J. M. Piau, "Experimental Study of Viscoelastic Effects in a Cylinder-Plane Lubricated Contact", J. Non-Newt. Fluid Mech., 13 79 (1983).

(11) Dowson, D. and C. M. Taylor, "Cavitation in Bearings", Ann. Rev. Fluid Mech., 11 35 (1979).

(12) Greener, J. and S. Middleman, "A Theory of Roll Coating of Viscous and Viscoelastic Fluids", Polym. Eng. Sci., 15 1 (1975).

(13) Greener, J., "Bounded Coating Flows of Viscous and Viscoelastic Fluids", PhD Thesis, Univ. Mass., Amherst, MA (1978).

References:(page 2)

(14) Horowitz, H. H. and F. F. Steidler, "Calculated Journal Bearing Performance of Polymer Thickened Lubricants", ASLE Trans., 3 124 (1960).

(15) Hsu, T. ,M. Malone, and S. Middleman, "Separating Forces in Blade Coating of Viscous and Viscoelastic Liquids", submitted (1984).

(16) Mensah, T. O.,"Enhancement of Strauss' Secondary Flow Mixing in Thin Film Commercial Reactors", Chem. Eng. Commun., 28 143 (1984).

(17) Metzner, A. B., E. A. Uebler, and C. F. Chan Man Fong, "Converging Flows of Viscoelastic Materials", AIChE Journal 15 750 (1969).

(18) Middleman, S., Fundamentals of Polymer Processing, McGraw Hill, N.Y. (1977).

(19) Pearson, J. R. A., "The Instability of Uniform Viscous Flow Under Rollers and Spreaders", J. Fluid Mech., 7 481 (1960).

(20) Saita, F. A. and L. E. Scriven, "Flexible Blade Coating", Paper presented at the AIChE Winter National Meeting, Atlanta, Georgia , March(1984).

(21) Sestieri, A. and R. Piva, "The Influence of Fluid Inertia in Unsteady Lubrication Films", J. Lub. Tech., 104 190 (1982).

(22) Shirodkar, P. and S. Middleman, "Lubrication Flows in Viscoelastic Liquids: 1. Squeezing Flow between Approaching Parallel Rigid Planes", J. Rheology, 26 1 (1982).

(23) Sullivan, T. and S. Middleman, "Roll Coating in the Presence of a Fixed Constraining Boundary", Chem. Eng. Commun., 3 469 (1979).

(24) Tung, T. T., K. S. Ng, and J. P. Hartnett, "Pipe Friction Factors for Concentrated Aqueous Solutions of Polyacrylamide", Letters Heat and Mass Transfer, 5 59 (1978).

(25) Walters, K. and D. M. Rawlinson, "On Some Contraction Flows for Boger Fluids", Rheol. Acta, 21 547 (1982).

APPENDIX A

MOMENTUM TRANSFER ARGUMENTS FOR AN INCREASE IN RESIDUAL FLUID THICKNESS WITH DECREASING BLADE LENGTH.

For the purpose of simplifying the present discussion, we consider the simplified geometry with zero curvature ($R=\infty$) and zero wiper blade angle shown in Figure A-1. Similar arguments apply to more complicated geometries.

Fluid entrained by the moving roll in our experimental apparatus approaches the wiper at a constant speed, equal to the roll speed. However, because of the no-slip condition at solid surfaces, the velocity of fluid making contact with the leading edge of the wiper becomes zero, which initiates the formation of a boundary layer as shown in Figure A-2. The thickness of the boundary layer , $\delta(x)$, is the distance over which viscous shear stresses, originating at the wiper surface, transfer momentum between the wiper and the fluid. Fluid outside of the boundary layer remains unaffected by the presence of the wiper. The boundary layer grows along the wiper, downsteam of the leading edge, and if the wiper is long enough, eventually fills the region between the wiper and the moving surface. For two parallel surfaces , one moving and the other stationary, the velocity profile is linear when it becomes "fully developed", and the distance required for this to occur is called the "entrance length (L_e)". Simple lubrication theory assumes that the

entrance length is zero and therefore, cannot account for "entrance effects", should they occur due to the developing boundary layer. For large wipers, when $L/L_e >> 1$, entrance effects are negligible, but as the wiper length decreases, the entrance region can become a significant fraction of the wiper length. We would like to have some estimate of how small a wiper must be in order for entrance effects to be significant and how these effects can influence the residual fluid thickness.

In an attempt to investigate entrance effects we consider the simple geometry shown in Figue A-1. From boundary layer theory (Bird, 1960 - pg.145) we know that the thickness of a boundary layer developing on the wiper can be approximated by

$$\delta(x) = 4.64 \sqrt{\frac{\nu x}{U}} \qquad \text{(A-1)}$$

with the velocity distribution

$$\frac{u}{U} = \frac{3}{2}\left(\frac{y}{\delta(x)}\right) - \frac{1}{2}\left(\frac{y}{\delta(x)}\right)^3 \qquad \text{(A-2)}$$

$$0 \le y \le \delta(x)$$

Assuming, that outside of the boundary layer fluid moves with the same velocity as the moving surface (u=U), the flow rate, Q, between the wiper and the moving surface can be written

$$Q = \int_0^{\delta(x)} U\left[\frac{3}{2}\left(\frac{y}{\delta(x)}\right) - \frac{1}{2}\left(\frac{y}{\delta(x)}\right)^3\right] dy + \int_{\delta(x)}^{H_o} U\, dy \qquad \text{(A-3)}$$

where $\delta(x) < H_o$. If the boundary layer thickness in the above expression is evaluated at the downstream edge of the wiper (i.e.

x=L), then the residual fluid thickness is given by

$$h = \frac{Q}{U} \tag{A-4}$$

Using the following dimensionless variables and substituting

$$\eta = \frac{y}{\delta(L)} \qquad \lambda = \frac{h}{H_o} \qquad Re = \frac{UH_o}{\nu}$$

Equations A-1 and A-4 into A-3, we obtain an expression for the residual fluid thickness, which is only valid as long as the boundary layer does not extend to the moving surface (i.e. $\delta(L) \leq H_o$).

$$\lambda = 1 - \frac{3}{8}\frac{\delta(L)}{H_o} = 1 - \frac{3}{8}(4.64)\left(\frac{L/H_o}{Re}\right)^{1/2} \tag{A-5}$$

The assumption that $\delta(L) \leq H$ constrains the blade length to

$$L \leq \frac{H_o Re}{(4.64)^2} \tag{A-6}$$

The actual wiper lengths for which entrance effects are significant is actually larger than this, because once the boundary layer reaches the moving surface, there is an additional transition region along which the velocity transforms into its fully developed linear profile.

Figure A-3 shows the effect of blade length, at a given Reynolds number, on the residual fluid thickness as predicted by

Equation A-5. According to the boundary layer arguments, the residual fluid thickness increases as the blade length decreases, when entrance effects are significant. The dotted line is an extension of Equation A-5 into the transition region of blade length, where boundary layer arguments are certainly invalid. Although we can not easily estimate the length of the transition region, it is obvious that simple momentum transfer arguments suggest that the residual fluid thickness increases when entrance effects are significant.

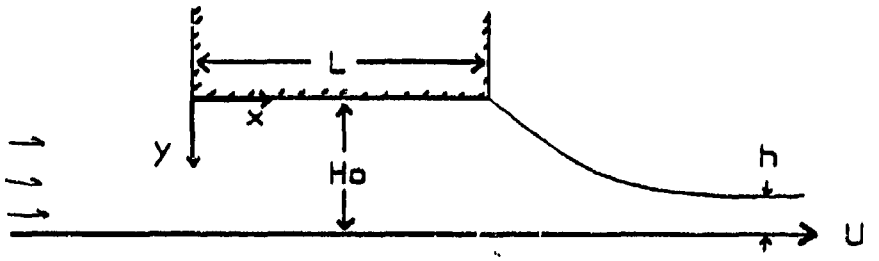

Figure A-1: Simple wiper geometry with zero curvature and zero wiper angle.

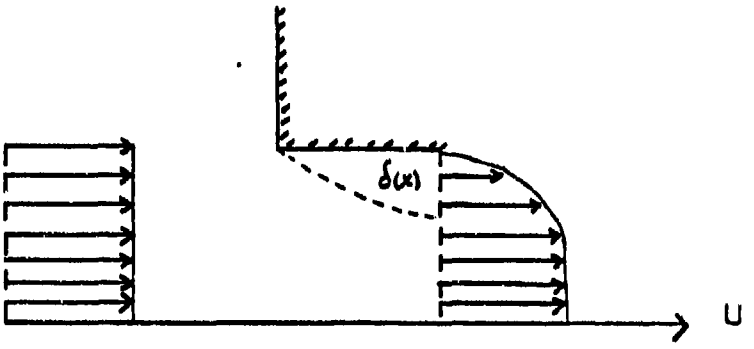

Figure A-2: Developing boundary layer at the leading edge of a wiper.

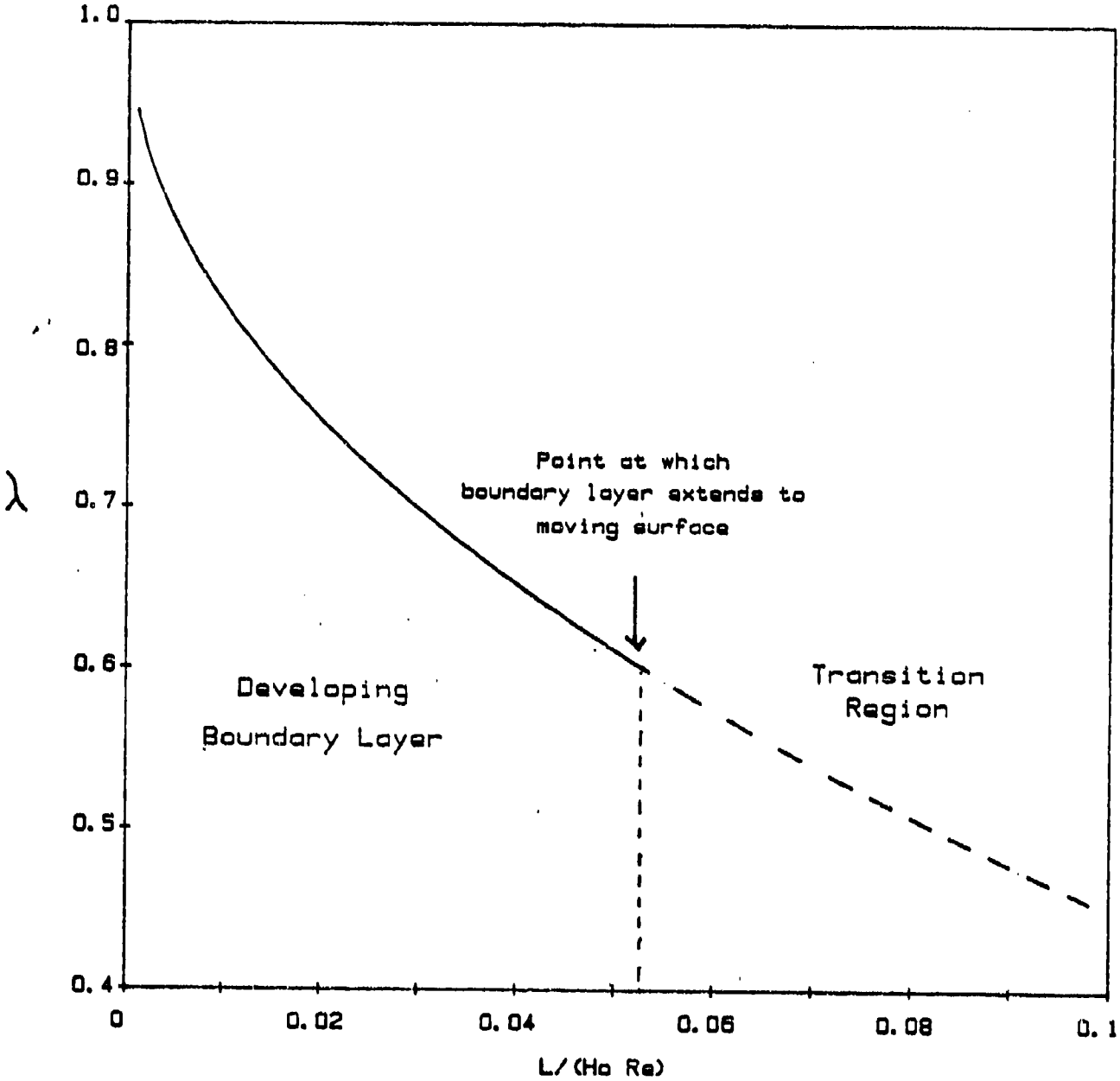

Figure A-3: Dependence of residual fluid thickness on blade length when entrance effects due to developing boundary layer are significant. Specific for geometry in Figure A-1.